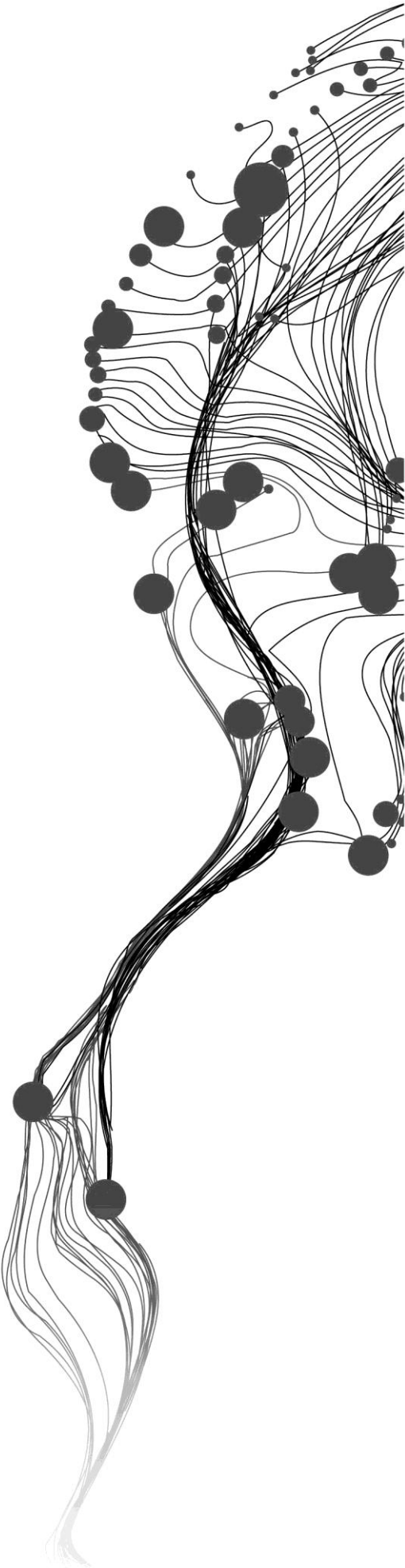# POLARIMETRIC MODELING OF LUNAR SURFACE FOR SCATTERING INFORMATION RETRIEVAL USING MINI-SAR DATA OF CHANDRAYAAN-1

KAUSIKA BALA BHAVYA
March, 2013

SUPERVISORS:

Mr. Shashi Kumar
Dr. V.A. Tolpekin

POLARIMETRIC MODELING OF LUNAR SURFACE FOR SCATTERING INFORMATION RETRIEVAL USING MINI-SAR DATA OF CHANDRAYAAN-1

KAUSIKA BALA BHAVYA
Enschede, The Netherlands, March, 2013

Thesis submitted to the Faculty of Geo-information Science and Earth Observation (ITC), University of Twente in partial fulfilment of the requirements for the degree of Master of Science in Geo-information Science and Earth Observation.
Specialization: Geoinformatics

THESIS ASSESSMENT BOARD:

Chair   : Prof. M.G. Vosselman
ITC Professor   : Prof. Dr. Ir. A. Stein
IIRS Supervisor   : Mr. Shashi Kumar
ITC Supervisor   : Dr. V. A. Tolpekin
External Examiner : Mr. Sanjay (DEAL, Dehradun)

DISCLAIMER

This document describes work undertaken as part of a programme of study at the Faculty of Geo-information Science and Earth Observation (ITC), University of Twente. All views and opinions expressed therein remain the sole responsibility of the author, and do not necessarily represent those of the faculty.

ABSTRACT

Mini-SAR of Chandrayaan-1 is the very first kind of hybrid polarimetric Radar flown outside the Earth's orbit. This sensor was employed to detect water ice deposits from the completely dark regions of the Moon. The hybrid polarimetric architecture of mini-SAR allows the measurement of the Stokes parameters of the backscattered signal. Decomposition techniques developed for this data include the m-δ and m-χ which have been used along with Circular polarization ratio (CPR) information to characterize the backscatter and look for water-ice deposits. This research presents an alternative to explore and study this data. H-α decomposition technique was used to extract the scattering information to study the physical properties of the targets. This approach utilizes the decomposition of Wolf's coherency matrix, derived from the Stokes parameters. The Eigen values and Eigen vectors estimated from the matrix decomposition are used in calculating the entropy (H) and mean alpha angle (α). The scattering mechanisms were characterized based on the combined interpretation of entropy and mean alpha angle. This technique was also employed to classify the targets based on their physical properties with the help of H-α plane. Surface scattering was found to be the dominant scattering pattern and most part of the lunar surface except the interior of craters were affected by this type of scattering. Double bounce reflections were difficult to categorize, but most of these patterns were encountered when the topography formed natural dihedral structures like the wall and the floor of the crater. The most important and interesting study was made with volume scattering component. High volume scattering was detected from inside the dark craters of the North Pole of the moon. The results were compared with the results obtained from the m-δ and m-χ decomposition techniques and CPR. The result of volumetric scattering from within the craters was validated against the Radar readings obtained from Greenland ice sheet and the icy planet of Europa. The high volume scattering could be attributed to anisotropic particles which could be buried ice or rocks. The H-α approach was successfully applied to hybrid polarimetric data to retrieve scattering information and in turn physical properties of the targets. Further improvements to this technique can derive the mean scattering mechanism from the Eigen values and Eigen vectors which can classify the targets in a proper manner.

Keywords: hybrid polarimetry, Stokes parameters, water ice deposits, Moon, H-α decomposition, CPR, scattering

ACKNOWLEDGEMENTS

TABLE OF CONTENTS

LIST OF FIGURES

LIST OF TABLES

1. INTRODUCTION

1.1. Background

Advancements in technology and science led to the application of remote sensing in the field of planetary sciences. Remote sensing deals with the collection of information about objects/phenomena without coming in contact with the object/phenomena under study. It utilizes the optical, infra-red and microwave regions of the electromagnetic (EM) spectrum to collect information. Remote sensing provides a unique perspective and presents various prospects for understanding different phenomena. The ability to provide temporal data, with high resolution capabilities makes remote sensing an ideal tool for planetary explorations.

Planetary sciences deal with the study of planets, their moons and planetary systems. The Moon is the Earth's only natural satellite and the Earth's nearest celestial neighbour. Lunar explorations and experiments have been conducted to study the nature, environment and general physiography of the moon. The "small step for man" in 1969 opened avenues for understanding mysteries of the moon. Microwave or RADAR (Radio Detection and Ranging) remote sensing offers an interesting insight and has many applications in the field of planetary sciences. A microwave is less affected by atmospheric conditions, and is sensitive to properties like surface roughness, wavelength used, moisture content and dielectric properties therefore providing a different set of information to look at [1], [2]. The polar regions of the Moon, especially the North Pole is completely dark, and the surface is heavily cratered. Studies state that these craters could be ideal regions where water ice could have been trapped [3]–[6]. Therefore, it makes Radar a preferable choice to collect information in these regions. Advanced Radar systems like Polarimetric SAR (Synthetic Aperture Radar) have enhanced capabilities to collect information.

A Radar system works by transmitting Radar pulses and receiving the backscattered signal. Imaging Radars are important in this field as they capture the electromagnetic radiation from the microwave region in the form of images. SAR sends Radar signals obliquely at right angles to the direction of flight towards the target. SAR is a side looking Radar system, which utilizes the system design to synthesize an extremely large antenna for generating high resolution remote sensing imagery.

1.1.1. The moon

The Moon is a celestial body which revolves around the Earth. It is the Earth's only natural satellite and the fifth largest satellite in our solar system. It is different from the Earth in many ways, especially in terms of atmosphere, physical and chemical surface properties. It was formed at around 4.5 billion years ago. There are many theories involving the formation of the Moon. One of the theories states that it was formed due to a giant impact between Earth and another Mars sized body. The Moon is a rocky planetary object heavily cratered on the surface

and flooded by lava flows. It was hit by meteors, comets and asteroids continuously, which led to the formation of regolith layer. Regolith can be termed as unconsolidated or loose rock material which more or less covers the entire surface or the underlying bedrock [7]. The regolith layer contains information that is necessary in order to understand the surface and environment of the Moon [8].Craters dominate all other features available on the Moon, other features being domes and cones, faults and graben. Our understanding of the lunar surface until now has been based on the data collected by various missions like the Galileo, Clementine and the lunar prospector and the samples of the regolith collected by missions like Apollo and Luna. The Moon contains various resources for space and Earth, water ice, minerals and metals being some of them. The Moon contains a record of information pertaining to planetary history, evolution and processes [9]. This information is not available on the Earth or elsewhere due to the dynamic processes which erode the surfaces continuously.

1.1.2. Polarization and hybrid polarimetry

Polarization which is a vital property of an EM wave, describes the direction of the oscillations of the transverse EM wave. An EM wave is composed of two time and space-varying components, electric and magnetic field components which at any point in time and space are orthogonal to each other and to the direction of propagation of the wave. Polarization, deals with the orientation of the electric field tracing a pattern as it moves in space (red line in Figure 1-1).

The amplitude, relative phase and the orientation of the two components of the electric field describe the type of polarization. A linear polarization is generated when the two components of the electric field vector are in phase and the orientation is at 45°. Changing the phase difference between two linearly polarized waves gives a variety of resultant polarizations. A circular polarization is formed when the relative phase is $\pi/2$ or $3\pi/2$ radians and the orientation is 45°. Phase differences in between these cases results in elliptical polarization.
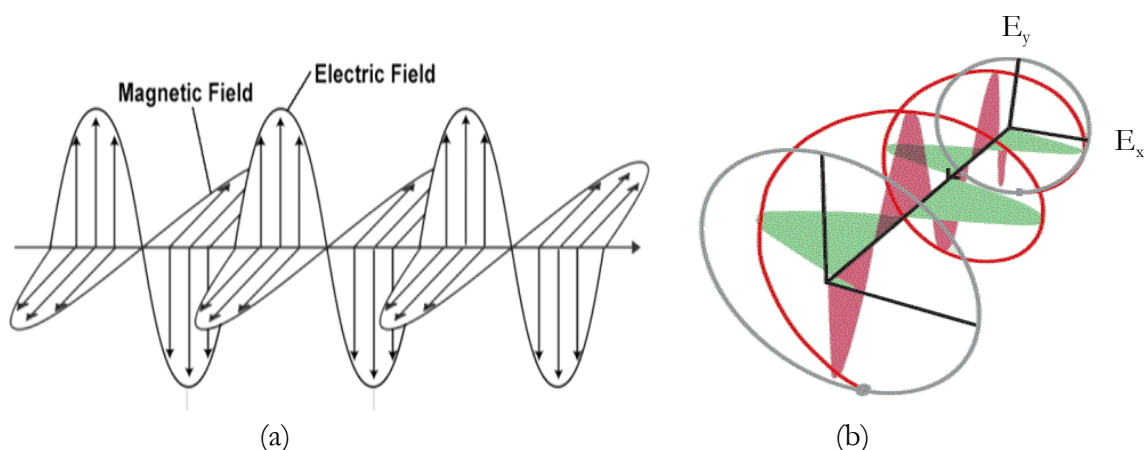
Figure 1-1: (a) Propagation of EM plane wave. (b)The horizontal (green) and vertical (red) components of the electric field vector combine to form the electric field vector (red); (b) represents the circular polarization. Source:(a)-[10], (b)- [11]

Polarimetric SAR architecture involves transmission and reception of Radar waves using a particular polarization. Depending on the type and number of polarizations used this architecture can be divided into different categories:

- Quad-pol or full polarimetry: Orthogonal dual transmission (H and V), coherent dual receive (HH, VV, HV and VH);

- Dual- pol and Compact polarimetry: Dual or single transmission and dual linear receive.

Hybrid polarimetry is a part of compact polarimetry where circular polarization is transmitted and two coherently linear polarizations are received. Conventionally in Radar astronomy and microwave lunar studies, circularly polarized waves were transmitted and dual-circularly polarized waves were received as, for example, in the Arecibo Radar telescope. Hybrid polarimetric data recorded by mini-SAR for the lunar surface offer similar data format as provided by Earth based Radar astronomical data [12]. When using hybrid polarimetric architecture the problems encountered in using quad-pol systems like mass, power consumption, limited area coverage, could be avoided. At the same time this architecture has an equal potential to provide most of the information, similar to that recorded by the quad-pol systems [13]. This type of architecture also provides various advantages as discussed by Raney [13].

1.1.3. Stokes parameters

A polarized wave experiences a change in its state of polarization when it interacts with a target. There are many ways in which the state of a polarized electromagnetic wave can be represented mathematically. The way in which it is represented should contain all of the information associated with the polarized wave. One such method of representation is by using Stokes parameters, developed by Gabriel Stokes [14]. These parameters are sufficient to describe the polarization state and other information (phase, intensity, degree of polarization, etc.) associated with the wave [1] . These parameters can be collectively represented by Stokes vector which is given by

$$\begin{bmatrix} S_1 \\ S_2 \\ S_3 \\ S_4 \end{bmatrix} = \begin{bmatrix} < |E_H|^2 + |E_V|^2 > \\ < |E_H|^2 - |E_V|^2 > \\ 2 \operatorname{Re} < E_H E_V^* > \\ -2 \operatorname{Im} < E_H E_V^* > \end{bmatrix} \qquad (1.1)$$

where S_1, S_2, S_3, S_4 are the four Stokes parameters, E_H and E_V are the received horizontal and vertical components of the electric field vector, Re and Im are the real and imaginary, $< >$ indicate ensemble averaging.

1.1.4. Decomposition techniques

Decomposition techniques help in interpreting the scattering information embedded in the polarization of a backscattered wave. Basically, polarimetric decomposition techniques work by splitting the polarized backscatter information from each SAR image pixel into a combination of different scattering mechanisms which help in the physical interpretation of the area under observation or the physical properties of the surface. These decomposition techniques can be divided into

- **Coherent decompositions**: These techniques are employed to study coherent targets or the so called pure or point targets, where the incident and scattered waves are completely polarized. These techniques are implemented using the scattering matrix. Some of the decompositions under this category are Pauli, Krogager and Cameron decompositions [14].

- **Incoherent decompositions**: The purpose of incoherent decomposition techniques is to characterize distributed targets. This is done by separating the coherency matrices used as target descriptors, into a combination of simpler matrices, which can be used for the physical interpretation of the target. Some of the different decompositions encountered in this category are the Freeman, the Huynen and the Eigen vector decompositions.

Other decomposition techniques which have been developed to fit the hybrid polarity data include the m-δ and m-χ decompositions. These techniques were implemented for different applications on earth and very recently on lunar data. The techniques consider the degree of polarization as a vital parameter for the decomposition [13], [15], [16]. Eigen value- Eigen vector based decompositions are also very useful in characterizing the polarized backscatter. This decomposition method derives the dominant scattering mechanism and its contribution in the total backscatter. In addition to this, with the application of this method classification of data is also possible [17].

1.2. Motivation and problem statement

Polarimetric SAR techniques when applied for planetary bodies can clearly exhibit the surface and subsurface properties [4], [18]. Hence it becomes a powerful tool for acquiring information. Space based and Earth based Radar observations of the moon have been carried out to investigate geology of lunar surface with an endeavour to study and map its surface [19]. The mini-SAR of Chandrayaan-1 mission was designed by employing hybrid polarimetric architecture for data collection. This is the very first kind of hybrid polarimetric Radar used outside the Earth's orbit [12]. Its objective was to acquire polarimetric data from the polar regions to detect water-ice deposits [20].

Studies [21], [22] have been conducted to model the lunar surface by considering different scattering mechanisms and modelling them to study the physical properties of the surface and subsurface. These studies were based on the data obtained from mini-SAR for water-ice detection. Water-ice detections were made on the basis of Circular polarization ratio (CPR), a

parameter derived from Stokes parameters. This was also used to model the lunar surface and to study its regolith layer. Until now, CPR is the employed tool for finding the water-ice deposits.

Scattering information can be retrieved using different methods. By using a decomposition model different scattering mechanisms can be retrieved, which provide information on the physical properties of the target. Eigen vector decomposition is an incoherent decomposition technique where covariance or coherency matrices are separated as a combination of simpler matrices for easier interpretation. The specular and diffused components of scattering mechanisms from the lunar surface include single (odd) bounce scattering, double (even) bounce scattering, and volume scattering. To retrieve the above scattering components from the data, which is in a relatively new format is a challenge. Information extraction based on a single parameter like CPR is often ambiguous. Although, decomposition models have been developed to study individual scattering mechanisms, their physical interpretation they might be constrained to the Earth's surface only. In addition to lunar surface being more complex and inaccessible, lack of proper data and evidence poses a challenge in the validation of the extracted information. Analysis of hybrid-polarized data by applying a decomposition technique, extracts most of the information available in the backscattered Radar signal, and can provide more accurate and reliable tool for modelling the lunar surface [21].

This research aims to explore the feasibility of applying an Eigen vector based decomposition technique (H-α) in order to extract scattering information. The information thus obtained, can be used for direct physical interpretation of the surface. By the application of this method three main scattering mechanisms single bounce, double bounce and volume scattering will be extracted. The retrieved scattering information can then be used in testing the reliability of CPR in looking for water-ice deposits and for modelling the lunar surface.

1.3.   Research objective

The objective of this research is to explore the scattering mechanisms derived by applying an Eigen vector decomposition technique on hybrid polarimetric data of mini-SAR for surface and subsurface information of the Moon.

1.3.1.   Sub-objectives
- To compare the m-δ and m-χ decomposition techniques for mini-SAR data
- To extract the scattering information using hybrid polarimetry based Eigen vector decomposition technique
- To evaluate the obtained results by using a Eigen vector decomposition technique to those obtained by using CPR and m-δ, m-χ decomposition techniques

1.3.2. Research questions

- What are the differences and similarities between the m-δ and m-χ decompositions and what is their success in retrieving the scattering information?

- How to apply the H- α decomposition technique to hybrid polarity data?

- Does the derived information enhance the findings of CPR?

- Does this technique help in providing better results in terms of amount of scattering information retrieved compared to CPR and the m-χ, m-δ decomposition techniques?

- How to validate the results obtained by using literature?

1.4. Structure of thesis

The thesis has been divided into 6 chapters. The first Chapter gives the overview of the research work, with introduction of the research, motivation and problem statement followed by research objective and questions. The second chapter on Literature review summarizes various studies related to the present research, which have been conducted. The third chapter gives information on the data used, the study areas selected and a detailed description of the adopted methodology. The obtained results and their explanation have been presented in Chapter four. Discussions on the results and the method adopted has been described in Chapter five and Chapter six concludes the work done and also provides recommendations.

2.   LITERATURE REVIEW

2.1.   SAR Polarimetry

An electromagnetic (EM) wave is composed of electric and magnetic field components. These components are always perpendicular to each other and also to the direction of propagation of the EM wave. Polarization of a wave refers to the behaviour (direction and oscillation) of the electric field vector as it travels. The polarization of a wave is characterized by the wave amplitude, orientation and ellipticity of the electric field vector [23]. These three variables define the type and intensity of the polarization. This property is useful for describing the type of scattering and the direction of propagation of the wave. In SAR systems, polarization is an important tool useful for different applications [24]. Figure 2-1 shows the different types of polarizations used in SAR systems.
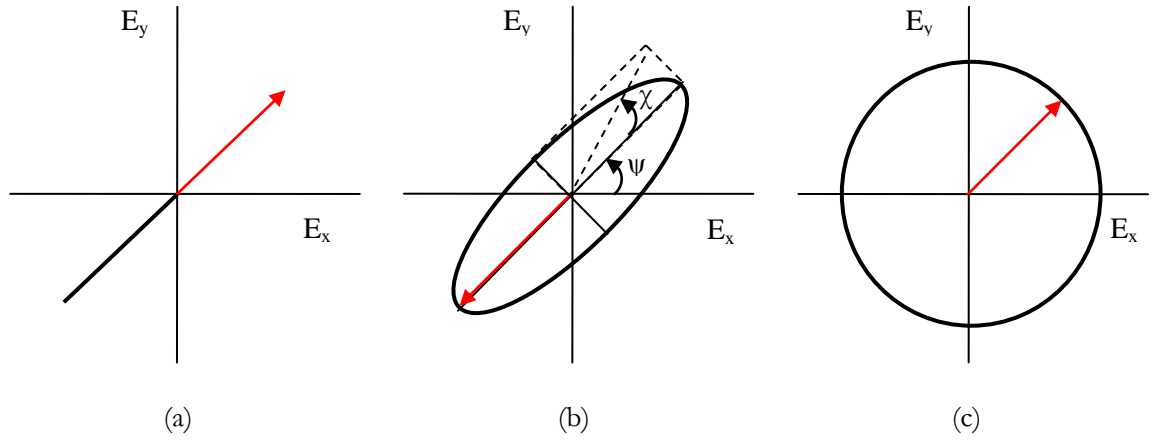
Figure 2-1: a) Linear, b) Elliptical and c) Circular polarization. The electric field vector is given in red. The length of this line is the amplitude of the wave.

The orientation angle (ψ) is the angle between the semi-major axes measured in an anti-clock wise direction from the positive horizontal axis. It can take values between 0º to 180º. The ellipticity angle (χ) describes the shape of the polarization ellipse [14]. This value ranges between +45º and -45º. In addition to orientation angle the relative phase (δ) is also important for describing the polarization. Relative phase is the phase difference between the horizontal and vertical components of the electric field vector. This parameter has not been shown in the figure. For linear polarization the relative phase is 0 or π with an orientation angle of 45º and ellipticity of 0. The linear horizontal and vertical polarizations occur when the components are in phase with orientation angles of 0, 180º and 90º and 270º respectively (Figure 2-1: (a)). When the relative phase is 90º a circle is formed from the polarization ellipse. In such a case the orientation remains at 45º the ellipticity angle becomes 45º forming a circular polarization (Figure 2-1: (c)). Therefore an ellipticity angle of +45º corresponds to a left circular polarization and -45º to right circular polarization [1]. Any other case in between the linear and circular polarizations corresponds to elliptical polarization [25] (Figure 2-1: (b)).

The Radar systems are designed such that they can transmit and receive one or many of the above mentioned polarizations. Since the polarization of the backscattered wave depends on the target, more than one polarization is employed to study the target properties [26]. Therefore, Radar antennas generally transmit either horizontal or vertical polarization and receive four different channels.

- HH – horizontal transmit and horizontal receive
- HV – horizontal transmit and vertical receive
- VH – vertical transmit and horizontal receive
- VV – vertical transmit and vertical receive

A system which is capable of receiving all the four polarization channels is known as quad-pol system or fully polarimetric. One which can receive only two of the above is known as dual-pol and single polarized if it can receive only one channel. The dual-pol and below are can be categorized as compact polarimetric systems. Apart from this circular polarizations are also used, especially in meteorological Radars and Radar astronomy. When circular polarization is transmitted there can be two types of receive.

- Same sense (Similar to the transmitted polarization)
- Opposite sense

A very recent development in compact circular polarimetry is hybrid polarimetry. An interesting possibility for improved SAR data collection implemented for the first time in Radar astronomy [12]. The system is designed to transmit circular polarization and receive linearly orthogonal polarizations; a new paradigm in Radar polarimetry. The mini-SAR and mini-RF Radars are examples of hybrid polarimetric systems.
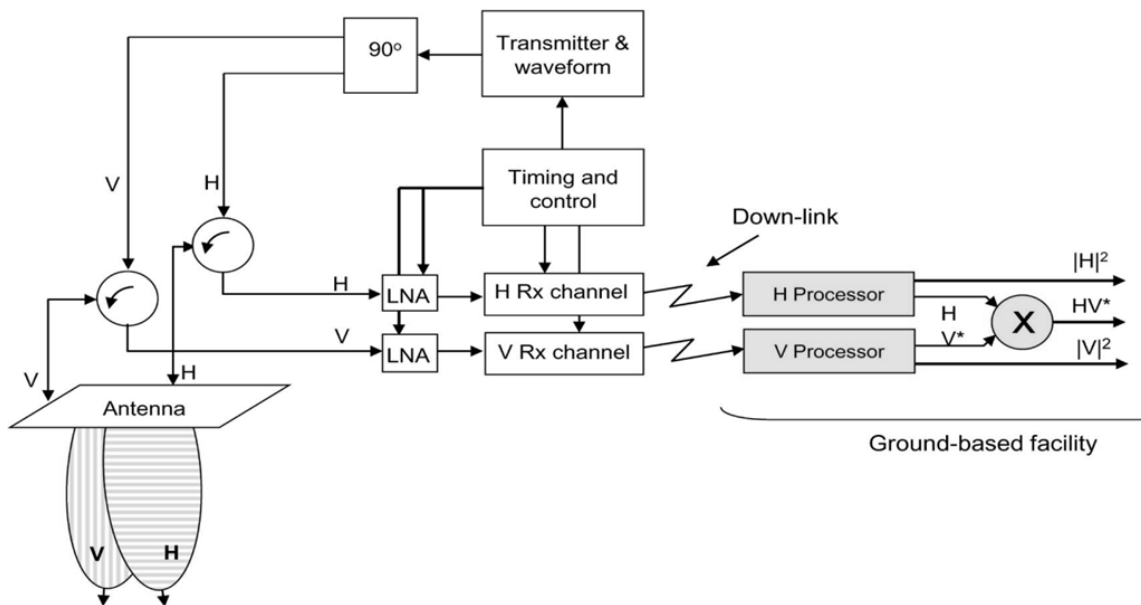
Figure 2-2: Hybrid polarimetric SAR architecture used in mini-SAR. Source :[13]

The hybrid polarimetric SAR systems transmit horizontal and vertical polarizations with a phase difference of $\pi/2$ so that circular polarization is generated [13]. Since the transmission is a single polarization, the system is dual polarized. It can either receive same sense or opposite sense polarization as in the Clementine bistatic Radar or it can receive two linearly orthogonal polarizations (Horizontal and Vertical) as in the case of mini-SAR and mini-RF Radars.

2.2. Stokes parameters and Coherency matrix

The polarization state of an electromagnetic wave can be given by Stokes parameters as shown in Equation (1.1). The four Stokes parameters are expressed in power terms rather than in terms of amplitudes and phases [1]. The first term S_1 is equal to the total intensity of the wave, S_2 describes the polarization state of the wave i.e. whether it is horizontal or vertical, S_3 and S_4 relate to the phase difference. S_3 describes whether the wave is linear, elliptical or circular while the fourth term describes the rotation or handedness (left or right handed). Only three of the four Stokes parameters are independent. The first term, the total power, is dependent on the other three parameters. Stokes parameters are important because they can also describe partially polarized waves in addition to the fully polarized waves. These Stokes parameters have a relationship with the angles of the polarization ellipse, as follows

$$\begin{bmatrix} S_1 \\ S_2 \\ S_3 \\ S_4 \end{bmatrix} = \begin{bmatrix} S_1 \\ S_1 \cos 2\psi \cos 2\chi \\ S_1 \sin 2\psi \cos 2\chi \\ S_1 \sin 2\chi \end{bmatrix} \tag{2.1}$$

For partially polarized waves $S_1 = \sqrt{S_2{}^2 + S_3{}^2 + S_4{}^2}$

Stokes parameters are the basic products derived from hybrid polarimetric architecture used in mini-SAR. Other parameters like the relative phase, ellipticity etc which are also known as Stokes child parameters can be derived from the Stokes parameters. The data represented in Stokes parameters is generally basis invariant which facilitates better interpretation and calculation of phase and ellipticity [25], [27].

Coherency matrix

The response from targets may not always have only a single scattering mechanism associated with them. Most of the targets are distributed targets i.e. they have mixed scattering responses due to the target properties and the system properties of the Radar beam incident on it. To effectively represent the complex scattering responses from distributed targets a coherency matrix is employed. It contains a set of averaged second order statistics (mostly variance and at times standard deviation) to describe a wave state and more commonly the backscattering information of a distributed target [23]. This is necessary in order to describe the physical properties of the target like surface roughness, dielectric constant, moisture, etc.

In the case of a hybrid polarimetric system (mini-SAR), the received signal is in four channels. Horizontal, vertical, the real and imaginary parts of the complex cross product between

horizontal and vertical components[12]. This leads to the construction of a 2×2 coherency matrix $[J]$ Equation (2.2) called the wave coherency matrix or Wolf's coherency matrix [23]. The Stokes vector for partially polarized waves is represented by this matrix and the elements of this matrix are in terms of intensity [28] The first matrix of $[J]$ is a general case of coherency matrix with orthogonal bases x and y; the second matrix corresponds to the transmission of left circular polarization denoted by L and reception in the H and V polarizations.

$$[J] = \begin{bmatrix} <E_x E_x^*> & <E_x E_y^*> \\ <E_y E_x^*> & <E_y E_y^*> \end{bmatrix} = \begin{bmatrix} <E_{LH} E_{LH}^*> & <E_{LH} E_{LV}^*> \\ <E_{LV} E_{LH}^*> & <E_{LV} E_{LV}^*> \end{bmatrix}$$

(2.2)

The coherency matrix $[J]$ given in terms of Stokes parameters can be represented as follows

(2.3)

$$[J] = \frac{1}{2} \begin{bmatrix} S_1 + S_2 & S_3 + iS_4 \\ S_3 - iS_4 & S_1 - S_2 \end{bmatrix}$$

A coherency matrix therefore is used for describing the target properties, embedded the polarization of backscattered wave. The dimension of the matrix depends on the system type. For example a fully-polarimetric system/ data format can be used for the calculation of a 4×4 coherency matrix, a dual-pol system 3×3 matrix and at times 2×2 matrix as in the case of hybrid polarimetry. It means that the dimension of the matrix depends on the number of polarization channels emitted and received by the Radar system. The matrix formed thus, is a complex Hermitian matrix with real values in diagonal elements [26]. The span of this matrix is equal to the total power of the wave (S_1).

2.3. Scattering

Scattering is a physical process in which an EM wave, incident on a target is redirected. The amount and nature of scattering depends on system properties like wavelength, polarization incidence angle used and target properties like shape, surface roughness, orientation angles and dielectric constant [29]. Therefore, surface features when illuminated by microwaves act differently based on the mentioned target and system properties. In this research surface scattering (single bounce), volume scattering and double bounce scattering have been considered.

Surface scattering takes place on the border surface between two different and homogenous media. In the case of a smooth surface specular reflection takes place. This directs the backscattered energy away from the sensor depending on the incidence angle. As the surface roughness increases in addition to the specular component, a diffuse scattering component is introduced [2]. When the surface is completely rough, there is only the diffuse component. The surface roughness is decided by a relation between the wavelength of the incident wave and the angle of incidence defined by Rayleigh criterion [1], [2]. According to Rayleigh criterion, a target is considered smooth if the standard deviation of surface roughness is less

than the ratio of wavelength to eight times the cosine of the incident angle. That means a target acts as a specular surface when the wavelength is greater than the characteristic magnitude of surface roughness defined by Rayleigh criterion. The lunar regolith acts as a specular surface for most of the part due to the high wavelength (12.6 cm) used in mini-SAR. In addition to this an incidence angle of 35° causes Bragg's type of scattering [30] . Surface scattering also occurs when the wall of the crater is perpendicular to the incident energy as shown in Figure 2-4.

Volume scattering takes place when the EM wave propagates from one medium to another. In volume scattering scenario, the energy is backscattered equally in all directions. The scattering component is completely diffuse. This is also known as random scattering. The backscatter contribution from volume scattering is considerably less due to the absorption and scattering by widely distributed particles within the targets [1]. Scattering by subsurface or soil layers, tree branches, snow layers are some examples of volume scattering. Permittivity changes in the medium of the wave propagation lead to volume scattering i.e. interactions from surface and subsurface. Volume scattering from lunar surface could arise from surface-subsurface interactions. The buried inclusions in the subsurface which may be the water-ice deposits or rocks in the central part of the crater give rise to volume type of scattering. The figure below shows the different types of volume scattering that is possible from the surface/ subsurface interactions.
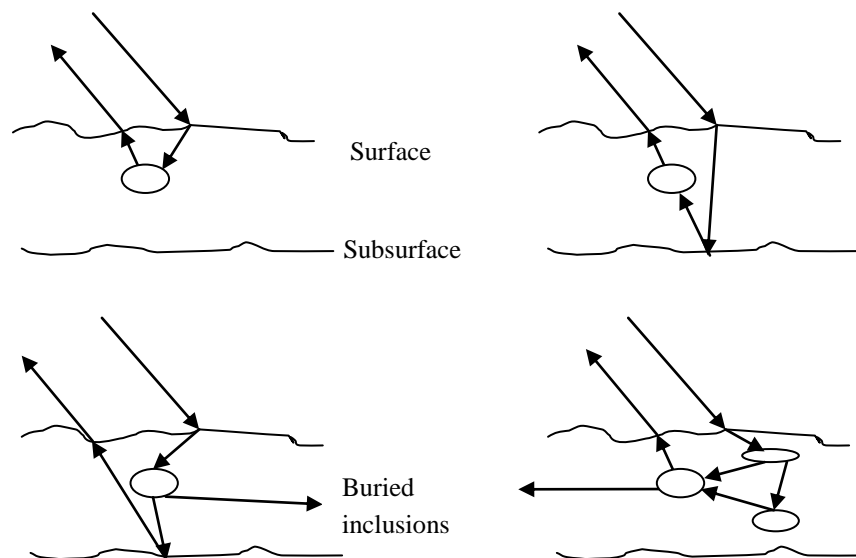
Figure 2-3:From top left (a) Volume scattering from buried inclusions, (b) Subsurface volume scattering, (c) Volumetric subsurface scattering, (d) Multiple scattering between buried inclusions.

Volume scattering is the major type of scattering that is possible from the lunar subsurface or the central part of craters. There can be various possibilities of volume scattering from the lunar surface

- Volumetric scattering from buried inclusions within the craters
- Subsurface volumetric scattering caused due to multiple interactions between the buried inclusions or particles, interactions between the surface and subsurface or scattering from the boundary of the subsurface etc.

Double bounce scattering occurs when the incident wave is backscattered in the same direction due to interaction with a dihedral or corner reflector. A case where the target acts as a double bounce reflector is when the wall and the floor of the crater from a natural dihedral structure causing the wave to return back in the same direction, with minimum transmission or absorption. There is minimum energy loss in this type of scattering as the backscattered energy is directed towards the antenna [31]. Double bounce reflections can also occur if rocks or other features on the surface are oriented in a manner that can cause two (or even number) phase reversals such that the backscatter is directed towards the Radar antenna. In such cases the phase of the backscattered wave is similar to the phase of the transmitted signal while the intensity might be more or less than the transmitted wave.
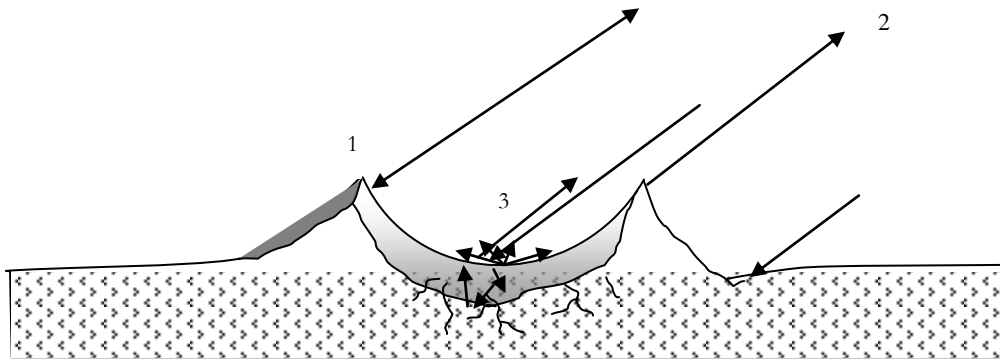
Figure 2-4: Scattering patterns from lunar surface crater. 1 represents surface scattering where the intensity of the backscatter is the highest. 2 shows double bounce scattering and the intensity of the backscatter is relatively high and 3 shows volume type of scattering where the contribution of backscatter is low due to diffuse type of scattering.

2.4. Studies on Lunar surface

Though studies on the lunar surface have started in the late 1900's, remote sensing has been applied in the field of planetary sciences only in first decade of the 21st century [8]. Since then scientists started experimenting with different techniques like gamma-ray spectroscopy, X-ray spectroscopy, optical, near infrared, thermal and finally Radar remote sensing. Optical studies on lunar surface have been carried out to study its surface, for crater detection studies and many other applications [32]. Other experiments using X-ray spectroscopy, thermal and infrared remote sensing have been conducted of studying the geology, minerals and the atmosphere of the moon [8]. The illumination condition at the poles renders optical imaging unsuitable [33]. Earth based Radar studies of the moon started with the Arecibo Radar telescope [3], [34]. The need to map the lunar poles was to confirm the results obtained by the Clementine mission which indicated the presence of water ice deposits in the cold trap (polar) regions of the moon [19]. This Radar utilized circular dual-polarization architecture to image the lunar surface. Radar studies have been employed thereafter for geologic studies [18]. The purpose and the renewed energy with which lunar studies have been taken up after a short break has been discussed in detail by Crawford *et* al [35].

Fa *et* al. [21] have developed a theoretical model of lunar surface considering five scattering mechanisms with the intention of interpreting data resulting from Chandrayaan-1 mini SAR. This model was developed using vector radiative transfer theory. The obtained model was then validated by comparing the measured polarimetric Radar coefficients with numerical finite difference time domain simulations and Earth based Radar observations. The study only considered five scattering mechanisms from the regolith. It also analyzed the possible polarimetric signatures of ice from the lunar surface, by considering four regolith models. In addition to this, the study also concluded that Circular Polarization Ratio (CPR) should not be the only parameter to be considered while looking for water-ice.

Raney *et* al. [16] developed an alternative decomposition technique to explore the presence of water-ice inside craters and also to examine the thickness of impact crater ejecta. For this, they chose two parameters; *m* (degree of polarization) and χ (the Poincaré ellipticity parameter), which are derived from Stokes parameters. The decomposition is aimed at the interpretation of lunar surface features with respect to single bounce scattering, double bounce scattering and randomly polarized components. This technique was developed to enhance the quality of information and interpretation provided by CPR. This technique was also able to distinguish lunar surface features based on their polarization properties.

Thompson *et* al. [22], developed a two component empirical model to study the Radar backscatter signatures for Chandrayaan-1 mini-SAR and LRO's mini-RF. Variations in specular and diffuse scattering components were assumed to estimate scattering differences associated with slopes, surface roughness, ice patches and thin regolith over ice. The Radar backscatter cross sections for earth based observations have been estimated to understand the measurements of mini-SAR and LRO This model has been used along with CPR to identify variations associated with possible ice deposits. Stacy and Campbell performed a similar study

to estimate lunar topography from polarized backscatter components, taking into account the slope and orientation angle [36]. Thomson *et* al. studied the roughness and slope characteristics from craters to help distinguish between ice bearing and non-ice bearing rough surfaces on the Moon [37].

Polarimetric properties of the lunar surface have been studied by Mohan *et* al. using mini-SAR data [20]. The CPR values in the polar and equatorial regions were compared to other parameters like degree of polarization (m) and delta (δ). Anomalously high CPR values attributed to planetary ice and increased double bounce scattering was found in some of the regions. These results when compared to the degree of polarization and relative phase showed different scattering mechanisms for different regions within and outside the craters of study.

The scattering properties of lunar equatorial regions using mini-SAR was conducted by Saran *et* al. [38]. In this study the backscatter intensities along with CPR, m, relative phase and Poincaré ellipticity parameter were used to conduct the analysis. The m-χ decomposition along with CPR information and backscatter intensities was found to be useful in characterizing the physical properties of the lunar surface. This study was aimed at providing information on the origin and (or) composition of lunar craters in the absence of information relating to age and composition of the lunar regolith.

The above mentioned studies were implemented on mini-SAR data. The key factor in all these studies was to either look for water-ice deposits or to study the scattering properties in order to estimate the physical properties of the lunar surface. In all the above studies CPR has been used as a traditional tool. Though one decomposition technique has been used to facilitate better interpretation of CPR, extraction of scattering information by using Eigen vector decomposition has not been implemented. This technique can retrieve most of the information and could aid in the detection of water-ice deposits.

2.5. Polarimetric Decomposition techniques for hybrid polarimetric data

The m-δ and m-χ decompositions are based on the Stokes parameters, m, δ and χ. The degree of polarization can be derived from the Stokes parameters(2.4). m is defined as the ratio of polarized power to the total power of the electromagnetic wave. This parameter is a significant distinguisher for characterizing the polarity of the backscatter. Polarity refers to the case of fully polarized, partially polarized or completely depolarized cases. The value of m is always between 0 and 1. Random or depolarized backscatter has a degree of polarization closer to the value of 0 while for polarized backscatter the value is closer to 1. Therefore, the value of degree of polarization for surface and double bounce scattering is closer to 1 and for volumetric type of scattering the value is closer or is equal to 0.

$$m = \frac{\sqrt{(S_2^2 + S_3^2 + S_4^2)}}{S_1} \qquad\qquad 0 \geq m \geq 1 \qquad\qquad (2.4)$$

The phase as such describes the stage of the cycle of the wave. The phase difference between the two components of the electric field vector describes the shape of polarization ellipse (linear, elliptical or circular). δ is measured in degrees. The relative phase (δ) is the angular difference of the phase between the two components of the electric field vector. δ is an indicator of double bounce scattering, and can be derived using the Stokes parameters as shown in (2.5). The type of scattering is indicated by the phase reversals. Double bounce scattering undergoes two phase reversals, leading to the reception of phase in the same sign as transmitted and with a difference of π.

$$\delta = \tan^{-1}\left(\frac{S_4}{S_3}\right) \qquad\qquad -180° \geq \delta \geq 180° \qquad\qquad (2.5)$$

The ellipticity parameter (χ) is a shape parameter which describes the degree to which the polarization ellipse is oval. The shape of the ellipse is governed by the magnitudes and relative phase between the horizontal and vertical components of the Electric Field vector [17]. It takes values between +45° and -45°. An ellipticity of χ= +45° corresponds to a left circular (LC) polarization and χ= -45° corresponds to a right circular (RC) polarization. χ is a sensitive indicator of even versus odd bounce scattering as calculated using (2.6). The ellipticity of the polarization is defined by this term and this corresponds to a parameter on the Poincaré sphere. The –ve sign in the equation corresponds to the transmission of left circular polarization of the mini-SAR.

$$\sin 2\chi = \left(\frac{-S_4}{mS_1}\right) \qquad\qquad -45° \geq \chi \geq 45° \qquad\qquad (2.6)$$

CPR has long been used as a primary indicator for representing scattering associated with planetary ice. This parameter is derived as shown in (2.7). CPR is greater than unity for features associated with volumetric water-ice or planetary ice deposits [16], [20], [38]. This is a

little ambiguous as strong double bounce reflections also have a CPR value which is greater than unity at times. This is because of the fourth Stokes parameter that has been considered which defines the handedness of the polarization. Double bounce and volumetric scattering lead to a greater numerator value than the denominator leading to a high value of CPR.

$$\mu_C = \frac{S_1 - S_4}{S_1 + S_4} \tag{2.7}$$

The coherency parameter or degree of linear polarization is closely related to the degree of polarization and is given by

$$\mu_L = \frac{\sqrt{S_3^2 + S_4^2}}{\sqrt{S_1^2 - S_2^2}} \tag{2.8}$$

2.5.1. m-δ decomposition

The m-δ decomposition technique has been used in [15] for land and oceanic applications for compact polarimetric data to check its robustness in differentiating between odd bounce and double bounce scattering. Degree of polarization, relative phase and orientation angle are the three parameters selected for the decomposition. Relative phase is a sensitive indicator between odd vs. even bounce backscatter especially when circular polarization is transmitted. This decomposition technique has been tested for applications like ship detection for circular transmission and linear receive data obtained from the Convair-580 and RADARSAT-2 fully polarimetric acquisitions. Though this technique is applicable for land and oceanic applications especially for fully polarimetric data, its application for hybrid polarimetric data is still being studied. The application of this decomposition technique to check its practical applicability for hybrid polarimetric data has been introduced by Raney *et al* for mini-SAR data [13], [39] . It has also been shown that this method is not advantageous as it could produce confusing results [16].

The m-δ decomposition can be denoted as follows as shown by Charbonneau [15]. The relative contribution of surface scattering is denoted by s, volume scattering by v and double bounce scattering by d.

$$s = \left[mS_1 \frac{(1+ \sin\delta)}{2} \right]^{\frac{1}{2}}$$
$$v = [S_1(1 - m)]^{1/2}$$
$$d = \left[mS_1 \frac{(1- \sin\delta)}{2} \right]^{\frac{1}{2}} \tag{2.9}$$

The classification of scattering into the above three components is solely dependent on the degree of polarization and delta. Delta being a sensitive indicator of double bounce scattering clearly distinguishes the difference between the surface and double bounce scattering when

circularly polarized waves are transmitted [13]. When delta is a positive value surface scattering is dominant and when it is negative double bounce scattering is dominant or has a greater contribution. As for volume scattering, it is the total power of the wave multiplied by the degree of depolarization, which gives the volume scattering. The degree of depolarization is consistent with random backscatter or highly diffuse scattering.

2.5.2. m-χ decomposition

Raney *et* al implemented the m-χ decomposition for the first time for hybrid polarimetric data to offer the Radar users who are unfamiliar with the relatively new data format, a method for data analysis [16]. In this decomposition method m, ellipticity parameter and orientation angle were used as the three parameters for the decomposition. This method proved to be useful in characterizing the lunar double bounce backscatter from surface scattering. On comparison with the m-δ decomposition this method was found to be efficient. This technique has also been used by Saran *et* al to study the scattering properties of the lunar surface, where this technique has significantly been highlighted [38].

The m−χ decomposition can be expressed as follows

$$s = \left[mS_1 \frac{(1 - \sin 2\chi)}{2} \right]^{\frac{1}{2}}$$
$$v = [S_1 (1 - m)]^{1/2}$$
$$d = \left[mS_1 \frac{(1 + \sin 2\chi)}{2} \right]^{\frac{1}{2}}$$

(2.10)

Here the differentiation of the scattering components depends on the ellipticity parameter. Clear differentiation between odd and even bounce scattering can made in this decomposition. This is due to the sign of χ which changes with respect to the different scattering components. The volume scattering component is similar that obtained in m-δ decomposition. Since this decomposition takes into account the handedness of the backscatter and ellipticity of the backscattered wave this becomes an effective technique.

2.5.3. H-α decomposition

This technique is based on the Eigen value analysis of the target coherency matrix $[J]$. Entropy (H), which is a measure of randomness relates to the un-polarized or the random components in the backscattered wave. H is used to assess the dominance of a scattering mechanism. Low values of entropy indicate that the target is weakly depolarizing and the dominant target scattering component is the Eigen vector corresponding to the largest Eigen value. If the entropy is high, the target is depolarizing and the full Eigen value spectrum should be considered for the interpretation. The value of H ranges between 0 and 1. The alpha parameter on the other hand describes the scattering mechanism or it is the scattering parameter. The value of alpha lies within 0°−90°. These two parameters are calculated from the Eigen values and Eigen vectors. The Eigen vectors describe the type of scattering pattern while the Eigen value gives the magnitude of the scattering [23], [40].

The 2×2 coherency matrix of the backscattered field for hybrid polarized data has 2 Eigen values and their corresponding Eigen vectors. The Eigen value problem is related to the matrix $[J]$ (coherence) to measure the full polarization state of the wave [23]. Since square matrices satisfy Hermitian properties, the matrix $[J]$ can be written as

$$[J] = [U_2].[D].[U_2]^{*T} = [\underline{w} \quad \underline{w}_\perp].\begin{bmatrix} \lambda_1 & 0 \\ 0 & \lambda_2 \end{bmatrix}.[\underline{w} \quad \underline{w}_\perp]^{*T} \tag{2.11}$$

Where λ_1 and λ_2 are the two Eigen values and $\lambda_1 \geq \lambda_2 \geq 0$. And

$$\underline{w} = e^{i\chi}\begin{bmatrix} \cos\alpha \\ \sin\alpha e^{i\delta_1} \end{bmatrix} \tag{2.12}$$

$\underline{w}$ is the Eigen vector which corresponds to the maximum Eigen value (λ_1). $[U_2]$ is the unitary matrix formed from the columns of the orthogonal Eigen vectors. Since each Eigen vector can be parameterized as in (2.13), $[U_2]$ can be derived as shown in (2.14). The two Eigen values are orthogonal i.e. $\lambda_1 + \lambda_2 = 1$.

Now that the Eigen values are normalized to unit sum, P_i is defined as shown below

$$P_i = \frac{\lambda_i}{\sum \lambda} \tag{2.13}$$

P_i can be interpreted as probabilities which represent the polarization states given by the Eigen vectors $\underline{w}$. The spread of these probabilities is represented by Entropy. The advantage of using probabilities is that, it provides an appropriate depolarization parameter (Entropy), which is 0 for completely depolarized components and 1 for maximum depolarization. In addition, the use of probabilities also presents a suitable basic invariant polarized parameter (scattering mechanism (α)) to represent the polarized component [23] .

The H-α decomposition uses normalized Eigen values denoted as probabilities for the interpretation [41]. Secondly taking into account that the second Eigen vector can be calculated from the first using the principle of orthogonality we can obtain an entropy/alpha parameterization of the coherency matrix. In this case of hybrid polarimetry or dual polarization the value of alpha can be represented on the Poincaré sphere [40]. The angles α and δ can be related to the angles ψ and χ, i.e. the state of a wave can be represented by either of these sets of angles.

The two normalized Eigen values depend on the degree of polarization and are defined in Equation (2.13). Entropy is then derived from the probabilities of the Eigen values and alpha from the Eigen vectors.

$$\lambda_{1,2} = 1/2(1 \pm m) \tag{2.13}$$

Entropy/Alpha decomposition is then derived for the interpretation of different scattering mechanisms as shown in Equation (2.14) below.

$$[J] = \begin{cases} [U_2] = \begin{bmatrix} \cos\alpha & -\sin\alpha e^{-i\delta} \\ \sin\alpha e^{-i\delta} & \cos\alpha \end{bmatrix} \\ [D] = (\lambda_1 + \lambda_2)\begin{bmatrix} P_1 & 0 \\ 0 & P_2 \end{bmatrix} \end{cases} \tag{2.14}$$

Equation (2.14) shows the decomposition in terms of normalized Eigen values and Eigen vectors. The matrix $[J]$ can further derived in terms of polarization and depolarization parameters H and α as follows

$$[J] \Rightarrow \begin{cases} \bar{\alpha} = P_1\alpha + P_2\left(\frac{\pi}{2} - \alpha\right) = \alpha(P_1 - P_2) + P_2\frac{\pi}{2} \\ H_2 = \sum_{i=1}^{2} P_i \log_2 P_i \end{cases} \tag{2.15}$$

The study of the scattering mechanisms thus derived can be performed by two methods. One method is the interpretation of H and mean angle alpha ($\bar{\alpha}$). The other is by using the Eigen values and Eigen vectors to derive the mean dominant scattering mechanism. In this research the scattering mechanisms are explored by interpreting the H and $\bar{\alpha}$ parameters. It is easier and reliable using these parameters as their values can easily be related to the scattering processes. For example mean angle alpha ($\bar{\alpha}$), can be related to the scattering processes as follows:

- *a→ 0*: The scattering corresponds to single-bounce scattering produced by a rough surface.
- *a→ π/4*: The scattering mechanism corresponds to volume scattering.
- *a→ π/2*: The scattering mechanism is due to double-bounce scattering.

2.6. Literature review summary

Studies conducted on the lunar surface have been dependent on CPR and m-χ decomposition techniques. It is necessary to look at the scattering mechanisms using a combination of tools as different decomposition techniques provide different results. Especially for areas (lunar surface) where validation is a challenge, different data analysis (decomposition) methods must be adapted in order to obtain better results. An alternative for extracting the scattering mechanisms from hybrid polarimetric data, other than using relative phase, ellipticity and CPR is the H-α decomposition. The scattering mechanisms are studied by the combination entropy and alpha angle values [42]. This approach could unambiguously distinguish different scattering types.

3. DATA AND METHODOLOGY

This chapter is divided into two sections; the first section describes the datasets used and the study area. The second section describes in detail the methodology adopted in order to achieve the research objective. A detailed methodology that has been followed is shown in the form of a flow chart in Figure 3-2.

3.1. Data and Study Area

The data used in this project is hybrid polarimetric data from Chandrayaan-1 mini-SAR. This was obtained in SAR mode and was formatted and stored in a planetary data system (PDS) compliant standards. The data product is comprised of four channels of data, Horizontal ($|LH^2|$) and the Vertical ($|LV^2|$) channels of the dual-polarized receiver, the Real ($LH.LV^*$) and Imaginary ($LH.LV^*$) cross-product of the complex H and V amplitudes. Each pixel in the image corresponds to 16 bytes, which equals to 4 byte floating point numbers for each of the channels. The data product was acquired in baseline SAR mode; the sensor operated in the S-band (wavelength 12.6 cm), with an incidence angle of 35º, and a ground range resolution of 150 m. The products selected for this project were processed till level 2, which are multi-looked (16 looks) SAR images in range and azimuth orientation with pixel values in beta naught, which have been radiometrically and polarmetrically calibrated. In addition the level 2 products are orthorectified and are re-sampled into with oblique cylindrical map projection [20], [43].

The data is available from the PDS geosciences node [44] and is in .img (Disk Image File, processed image) format. It is supported by a .txt (unstructured text data) file, a parameter file listing the parameters and values used in the calibration. A KML file is also provided which gives the foot print of the area imaged.

Dataset description	
Sensor	Mini-SAR
Incidence angle	~35º
Swath	8 km
Azimuth resolution	150 m
Polarization	Left circular transmit, Receive coherent linear H and V
Slant range resolution	≥ 86 m
Wavelength	12.6 cm
Polarization	Left circular transmit, Receive coherent linear H and V

Table 3-1: Description of the dataset

Two study areas have been selected in order to carry out the research. The first study area is of the Erlanger crater. The dataset selected for the first study area (Erlanger crater) is **fsb_01299_2cd_oiu_86n326_v1.img**. This dataset has a resolution of 118 m per pixel and covers the region of Erlanger crater which is located at 86.94°N 28.62°E and is nearly 10 km in diameter. Erlanger is a north polar crater situated between the very large craters Peary and Byrd. Most part of the floor of this crater is in complete darkness due to its closeness to the North Pole. This crater has been of interest as the images from mini-SAR and mini-RF suggested unusual scattering properties from the interior and exterior of the crater [45], [46].

The figure below shows the lunar North Pole in a stereographic projection. Study area two, part of Rozhdestvenskiy crater selected in this research is a small area. The region highlighted in the green box on the lunar image is the whole of Rozhdestvenskiy crater which is about a 100 km. The mini-SAR image shown on the right is the intensity image which covers about 8×20 km area of the Rozhdestvenskiy crater.
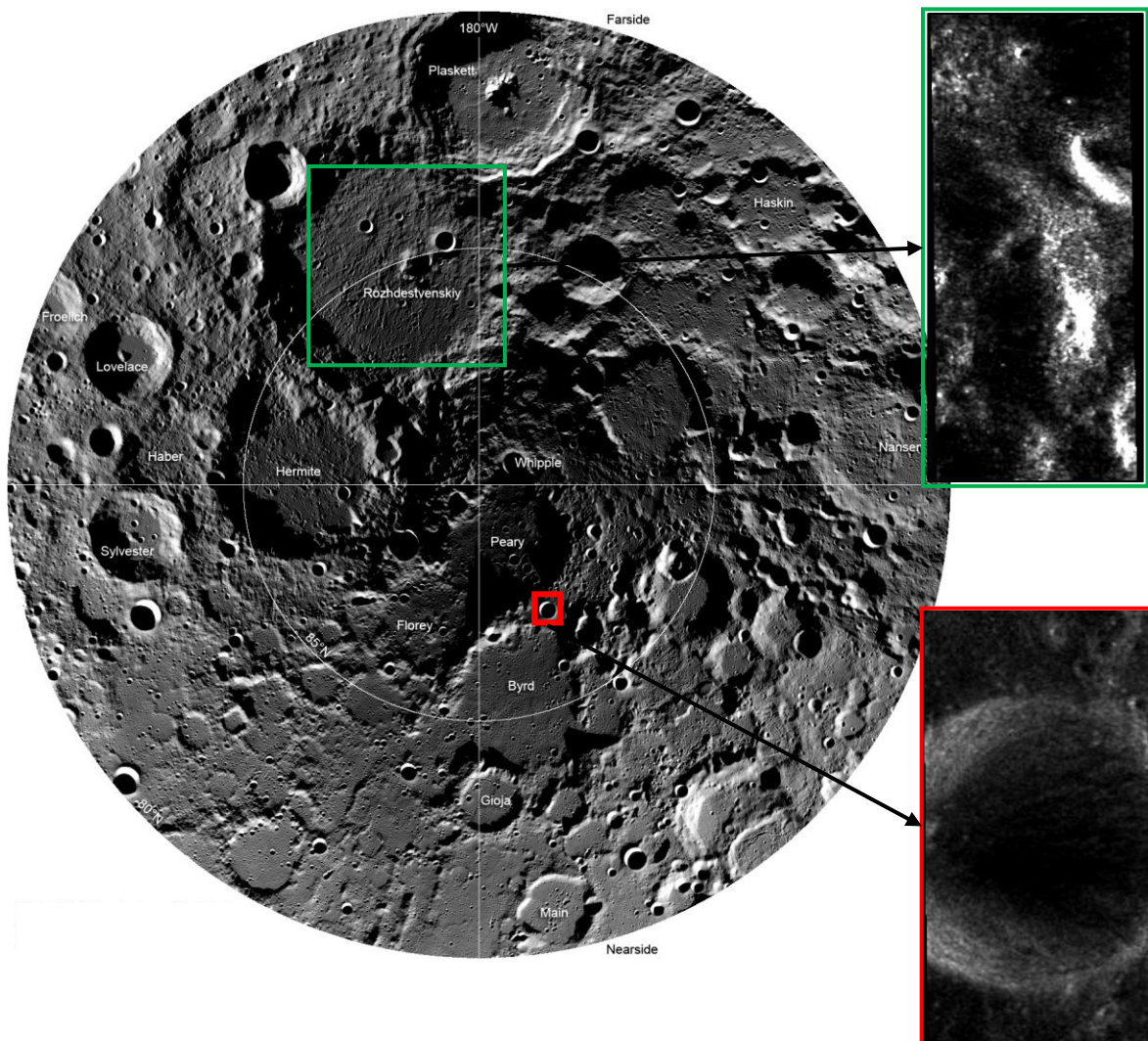
Figure 3-1: The image shows Mosaic of the Lunar North Pole obtained by LROC WAC mission. Source: [41]. Study area 1; Erlanger crater highlighted with a red box on the image of the Moon. Study area 2; a small part of the Rozhdestvenskiy crater has been selected which is shown in a green box on the right.

The second dataset is **fsb_01188_2cd_oiu_85n086_v1.img** which is a small part of the Rozhdestvenskiy crater. Secondary craters on the floor of Rozhdestvenskiy have been selected for this project.

3.2.   Methodology
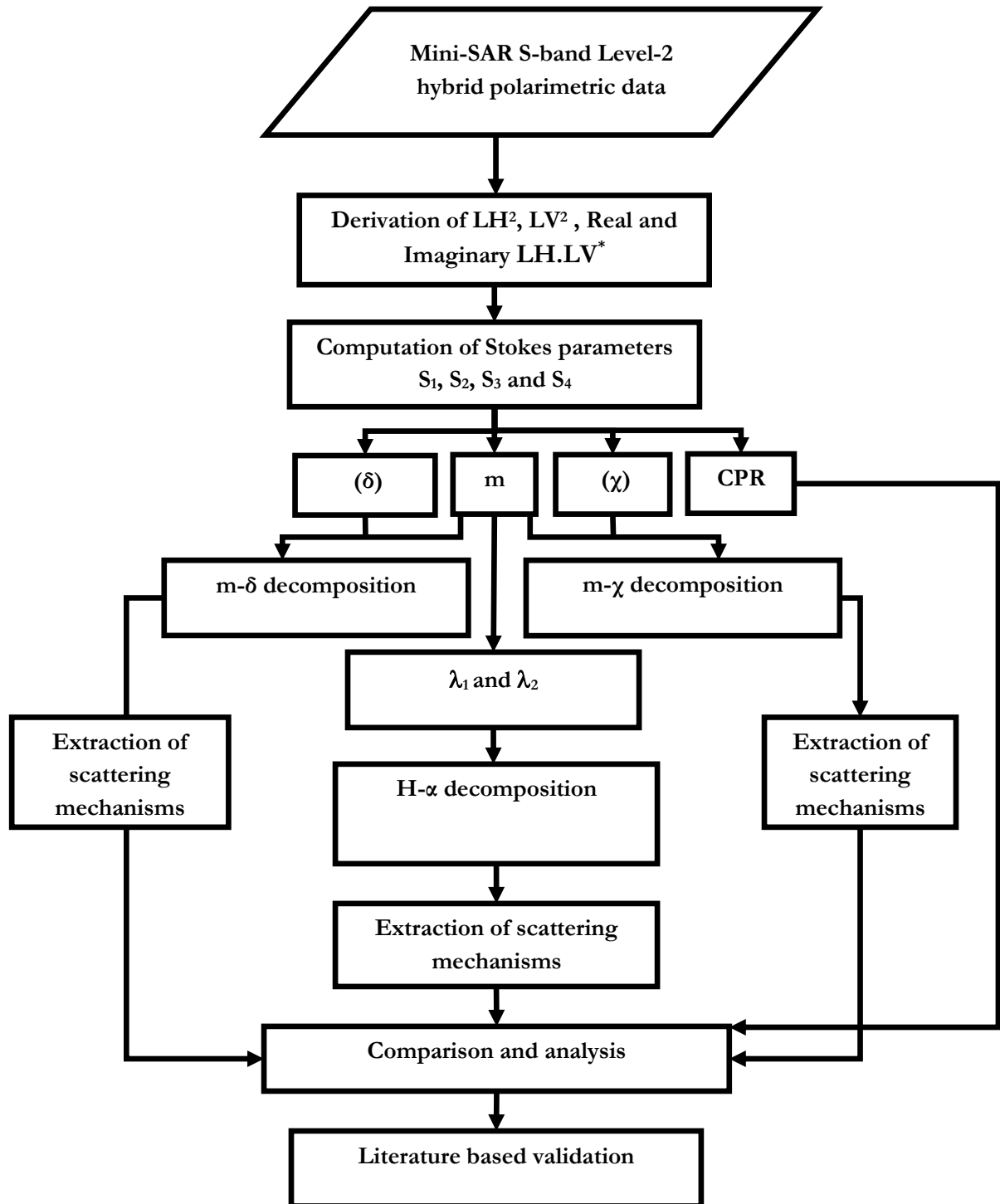
Figure 3-2: Flow diagram of the methodology adopted.

The methodology adopted to achieve the objective of the study is shown in Figure 3-2. The data in the four polarization channels is first converted into the Stokes parameter files. Then other parameters like degree of polarization, relative phase, ellipticity and CPR are calculated. The next step is to implement the decomposition techniques and extract the scattering mechanisms from the results. The m-δ and m-χ decomposition techniques which have already been used by Charbonneau *et* al.*,* Raney *et* al. and Saran *et* al. are implemented [13], [14], [35]. The next step proceeds with the main work, which is the derivation of the Eigen values and the Eigen vectors from the parameter m. Then Entropy-alpha decomposition method derived to fit the data format is to be applied from which the scattering parameters are retrieved once again. Finally, analysis and comparison of the obtained results of all the decompositions and CPR is to be conducted.

3.2.1. Derivation of Stokes parameters

The process starts with the derivation of the Stokes parameters from the data from which follow other parameters like degree of polarization (m), relative phase (δ), Poincaré ellipticity parameter (χ), CPR etc, which are used in the decomposition methods. The data provided consisted of the intensity images for the horizontal, vertical and the real and imaginary components of the complex cross power intensity between horizontal and vertical receive. This was sufficient to calculate the 2×2 coherency matrix and the Stokes parameters. The Stokes parameters were derived from the given data set by incorporating the Stokes equation defined in Chapter 1. The following equation corresponds to the hybrid polarimetric architecture of mini-SAR. *L* stands for transmission left circular polarization and *H* and *V* are for horizontal and vertical polarizations that are received.

$$\begin{bmatrix} S_1 \\ S_2 \\ S_3 \\ S_4 \end{bmatrix} = \begin{bmatrix} < |LH|^2 + |LV|^2 > \\ < |LH|^2 - |LV|^2 > \\ 2\,\mathrm{Re} < LH.LV^* > \\ -2\,\mathrm{Im} < LH.LV^* > \end{bmatrix} \tag{3.1}$$

where, * denotes complex conjugate.

(a)

(b)

(c)

(d)
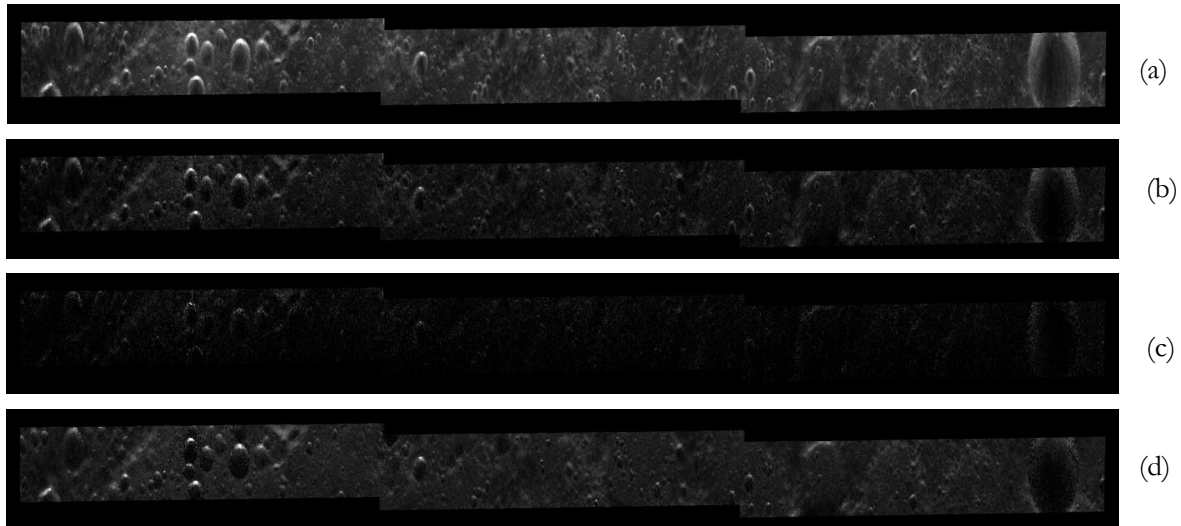
Figure 3-3: (a) S1 (b) S2 (c) S3 and (d) S4 images generated from 4 channel data

3.2.2. Calculation of Delta (δ), Chi (χ), degree of polarization (m) and CPR.

The Stokes child parameters i.e. the parameters estimated from the Stokes parameters are to be calculated next as they form the basis of further calculations and analysis. CPR, m, δ and χ are calculated using the Equations (2.7), (2.4), (2.5) and (2.6) respectively. The images obtained with the mentioned calculations are shown in Figure 3-4 and Figure 3-5. These images are of the Erlanger crater, the major focus area of study in this thesis. The obtained parameters (δ, χ and m) are used in the decomposition techniques that are to be applied in the next step.

(a)   (b)
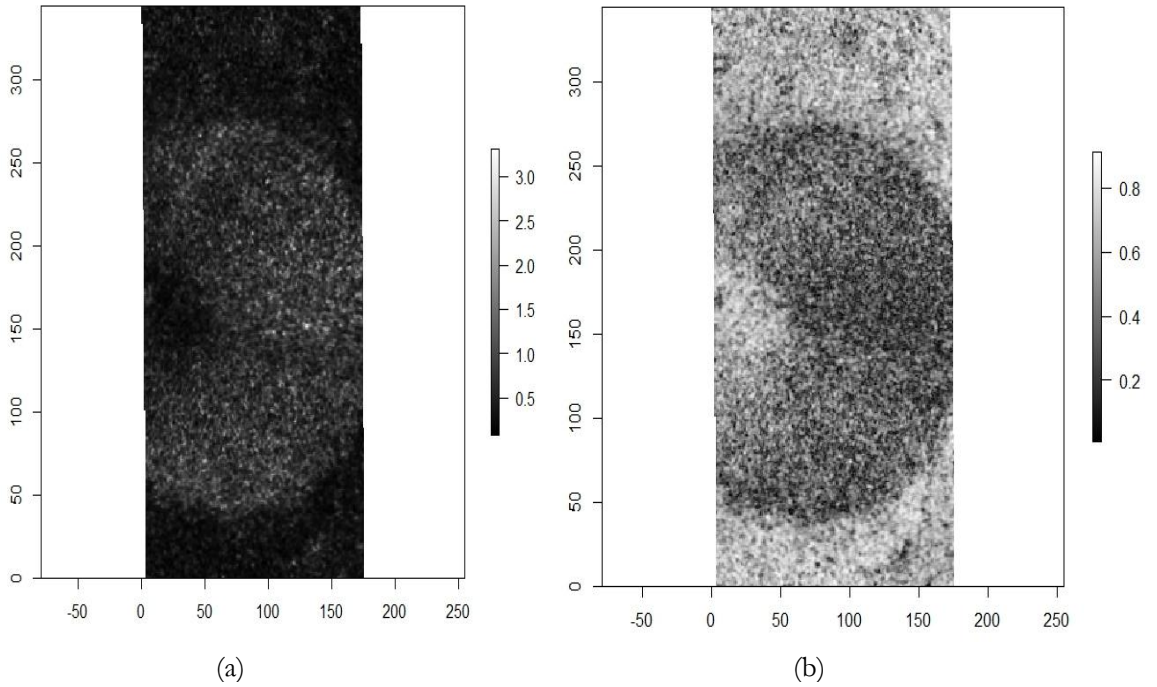
Figure 3-4: (a) CPR and (b): Degree of polarization images

(a)   (b)
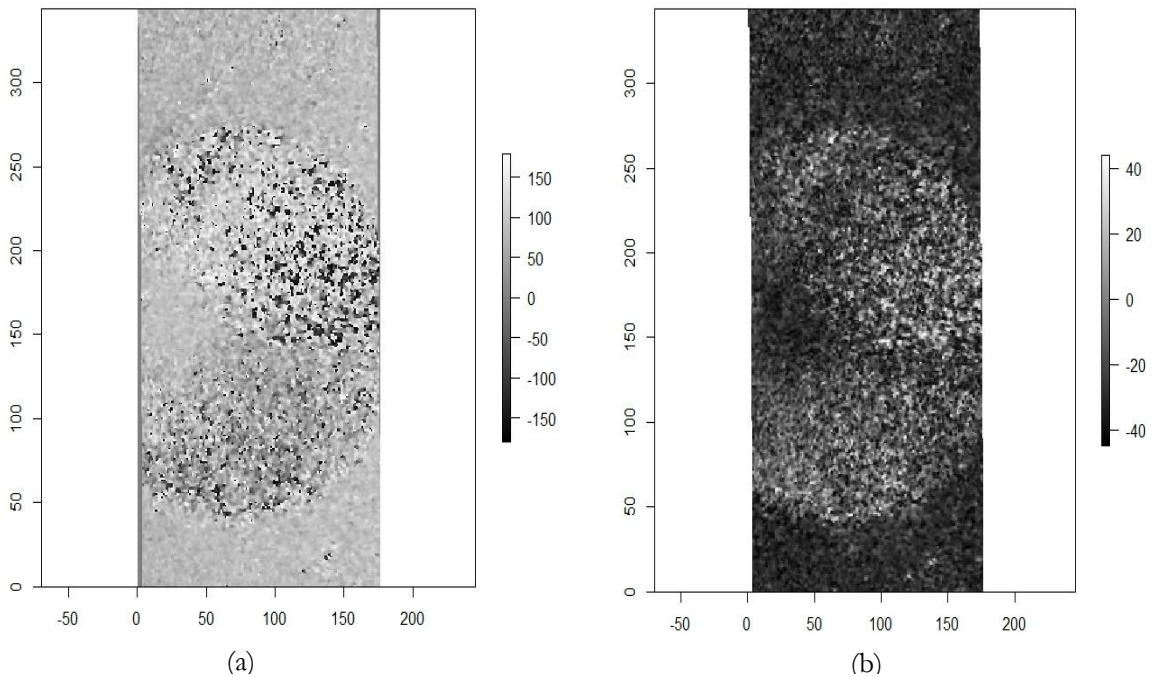
Figure 3-5: (a) Delta (δ) and (b) Chi (χ) images

3.2.3. The m-δ, m-χ decompositions and CPR

The m-δ and m-χ decompositions and calculation of CPR are based on the Stokes parameters. The parameters m, δ and χ which are derived from the Stokes parameters are used in the decompositions while S_1 and S_4 have been used to calculate CPR. These decompositions were implemented using Equations (2.9) and (2.10) described in Chapter 2. Scattering information will be retrieved from the decompositions. This information would then be compared among different decomposition techniques applied. In addition to this CPR information would be used as a supplement in analyzing the results.

3.2.4. H-α decomposition

This method is based on Eigen value analysis. λ_1 and λ_2 values are used to calculate the entropy and the mean alpha angle (Chapter 2, Equation (2.14), (2.15)). The first alpha input for the calculation of mean angle alpha is derived from the Stokes parameters which represent the polarization state of a plane wave [28]. The value of alpha is derived as

$$\cos 2\alpha = \left(\frac{S_2}{S_1}\right) \tag{3.2}$$

This value of alpha is further used with the Eigen values for calculating the Eigen vectors and for performing the H-α decomposition as explained in Chapter 2.

3.2.5. Comparison and analysis of m-δ, m-χ, H-α and CPR

The next step in the process is the analysis of the 4 methods to find out which technique gives better results quantitatively and qualitatively. The information regarding the scattering mechanisms obtained from different techniques will be compared and analyzed with the results of CPR.

- **Sampling plan**

For data analysis, results are analyzed, by selecting small samples from the outputs obtained from applying the decomposition methods. Focus will be on the Erlanger crater which has been selected as the main study area. Samples containing 120 pixels are selected based on random sampling on the basis of location. Therefore, pixels from within and outside the crater will be used in the analysis to study the different type of scattering mechanisms and their intensities.

- **Data analysis techniques**

    i.   Transects/ Box plots

Transects for regions within and outside the crater are created. The backscatter value of these pixels for various scattering mechanisms are then plotted against each other to see how these components vary for different decomposition methods. In addition, box plots are also plotted for the selected samples. The contributions from scattering mechanisms for different decomposition techniques will be analyzed for the same set of pixel samples. Variations in

surface and double bounce scattering intensities are calculated in terms of mean and standard deviations.

      ii.   CPR based analysis of volume scattering derived from applying decomposition techniques

Volume scattering derived from H-α method and m-χ and m-δ decomposition methods are investigated with the help of CPR. CPR values greater than unity, can be associated with volumetric ice deposits, as well as strong double bounce scattering. If this information is overlaid on the volume scattering contribution from different decomposition techniques, then actual areas contributing to volume scattering could be identified. Then this type of scattering could also be attributed to water-ice deposits on the lunar surface.

3.3.   Validation

Validation of the results is carried out by comparison of the scattering mechanisms using a literature based approach. Radar signatures similar to those found on the icy planets, or satellites like Europa, Callisto, Ganymede, and the Moon have been documented on the Earth's surface. The observations were recorded over Greenland ice sheet. Circular polarization and linear polarization ratio readings have been collected at 5.6, 24 and 68 cm. These Radar echo readings from Greenland ice sheet [47], [48] would be used to verify the volumetric scattering response (consistent with water-ice deposits) from the lunar surface. Comparative analysis would be conducted to check whether the scattering responses correspond to actual physical features present on the lunar surface.

4. RESULTS

This chapter presents the results obtained in this research work. First, the results of the major steps in methodology are presented along with the observations, followed by data analysis to examine the results and their interpretation.

4.1. *m*-δ decomposition

The results of the *m*-δ decomposition and individual components of the three scattering mechanisms (surface scattering, double bounce scattering and volume scattering) for the Erlanger crater (study area 1) are given in Figure 4-1 and Figure 4-2 respectively. The three scattering mechanisms have been displayed with the help of RGB colour planes. The intensity of each colour is given by the relative contribution of the components. The secondary colours (Cyan, Magenta and Yellow) represent a mix of scattering patterns. For example, magenta is a combination of double bounce and surface scattering as can be seen from Figure 4-1: (b).
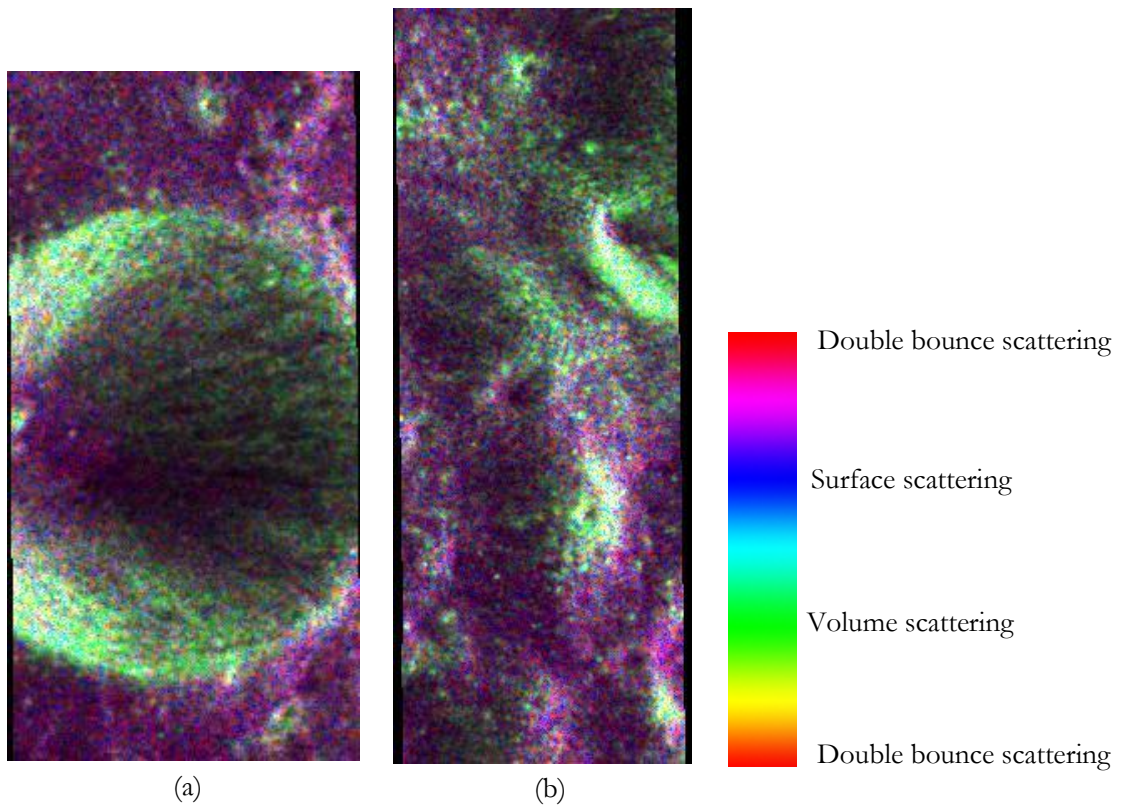
Figure 4-1: m-delta decomposition (a) for study area 1 (Erlanger crater) and (b) study area 2 (floor of Rozhdestvenskiy crater) followed by the interpretation for the decomposition. Red stands for double bounce scattering, blue for surface scattering and green represents volume scattering.

From the decomposition image Figure 4-1 (a), a combination of surface and double bounce scattering is dominant for most part, while volume scattering occurs in regions where craters are present. In Figure 4-1(b), volume scattering is observed from secondary craters, while a mixture of surface and double bounce scattering can be observed from the floor of the crater.

On analyzing the Erlanger crater, the contribution from volume scattering component was found to be more followed by a combination of surface and double bounce scattering components. Surface scattering was observed from the steep walls of the crater, where the incoming wave is scattered back directly towards the sensor. Double bounce scattering on the other hand has been observed at the edges where the surface and the crater wall form a natural dihedral. The contribution from volume scattering component form this decomposition was higher in and around the craters, especially where the degree of polarization is very low. The surface could be very rough with respect to the 12.6 cm used or absorption could be talking place which is leading to diffuse scattering pattern, and in turn high volume scattering. High volume scattering from around the craters in (b) can be attributed to fresh craters. This is because the ejecta from newly formed impact craters is composed of rock particles and materials which form a very rough surface, leading to diffuse scattering phenomenon.

(a)   (b)   (c)
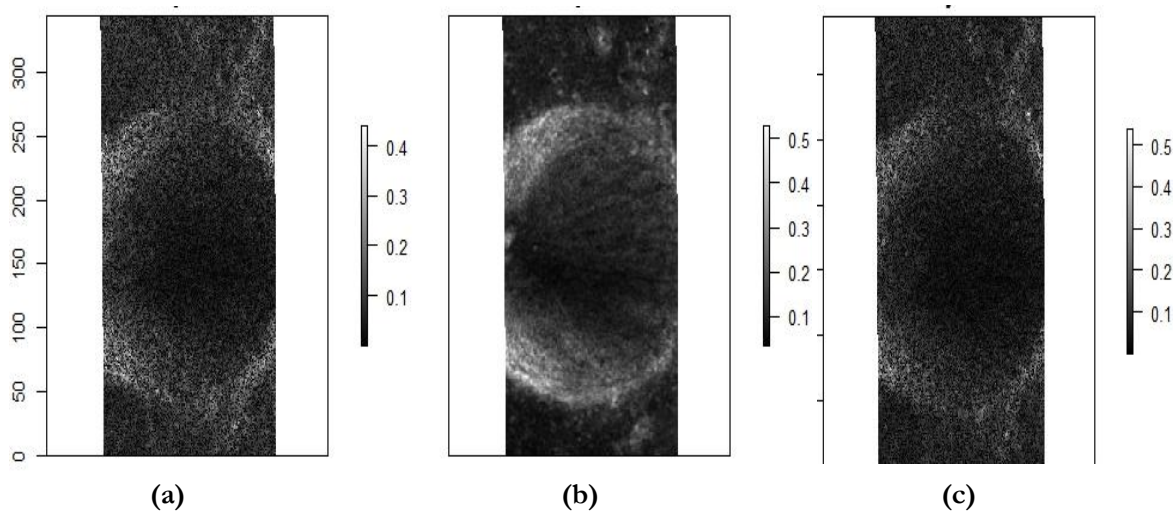
Figure 4-2: Individual scattering components for m-delta decomposition (Study area 1). The relative contribution from (a) surface, (b) double bounce and (c) volume scattering add up to the total backscattered power.

Upon closer observation of the individual components of scattering, it has been found that the major deciding factor of the type of scattering is the relative phase. This can be established from the formula used for the decompositions. When the relative phase value is negative it leads to double bounce scattering and a positive value leads to surface scattering. Most of the surface scattering component is due to the contribution of Bragg's type of scattering. This is a

common phenomenon experienced, when the incidence angle is around 35°. The mean value of surface scattering component was found to be 0.07 and for double bounce scattering it was 0.08. As for volume scattering the mean value was observed to be 0.13. The dominance of volume scattering in this region may be due to the roughness and the materials present in and around the crater. The dominance of volume scattering in this region may be due to the roughness and the materials present in and around the crater.

4.2. m-χ decomposition

The results of the m-χ decomposition for the two study areas are shown in Figure 4-3. The interpretation of the colour coding is similar to the m-δ decomposition. This decomposition technique produced better results by differentiating the scattering processes in an enhanced manner. Surface and double bounce scattering have been singled out without ambiguity. On analyzing the Erlanger crater, strong backscatter responses were observed from the crater walls which could have been perpendicular to the incoming incident wave. These strong responses correspond to surface scattering and sometimes double bounce scattering where the natural dihedrals on the surface could lead to stronger backscatter response than the incident wave. The volume scattering component can be distinguished visually and this occurs along the walls towards the centre of the crater. Volume scattering mechanism is dominant for most part of the interior of lunar craters.
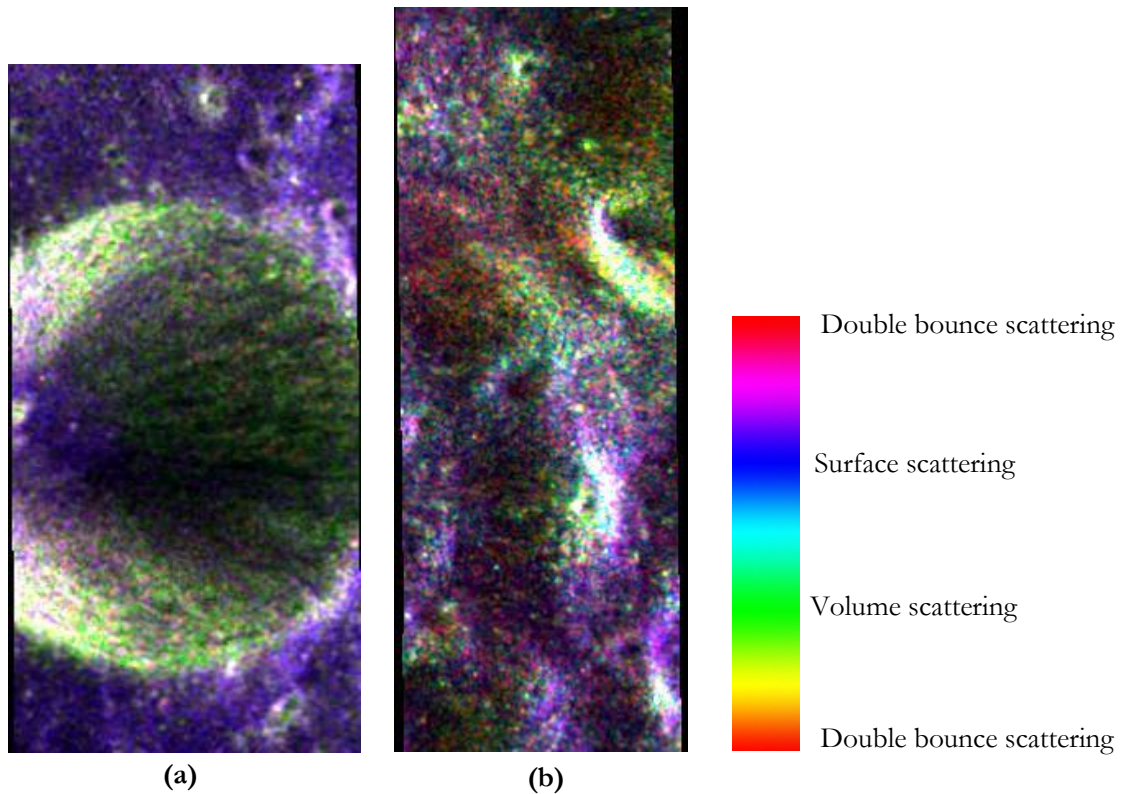
Figure 4-3: m-χ decomposition images for (a) Erlanger crater and (b) Study area 2. Red is for double bounce scattering, blue for surface scattering and green stands for volume scattering.

In Figure 4-3 (b), the topography is undulating with basins and dome like features and hence the scattering from this area is a combination of odd bounce and double bounce scattering. The volume scattering component remains the same, i.e. pertaining to the interior parts of the crater and impact crater ejecta.

Figure 4-4 shows the scattering components derived from the m-χ decomposition; double bounce, volume and surface scattering respectively. The mean intensity of surface scattering is around 0.11 for the Erlanger crater, while double bounce scattering is around 0.04. The sign of the ellipticity parameter plays a crucial role in categorizing the scattering mechanisms.

(a) **(b)** **(c)**
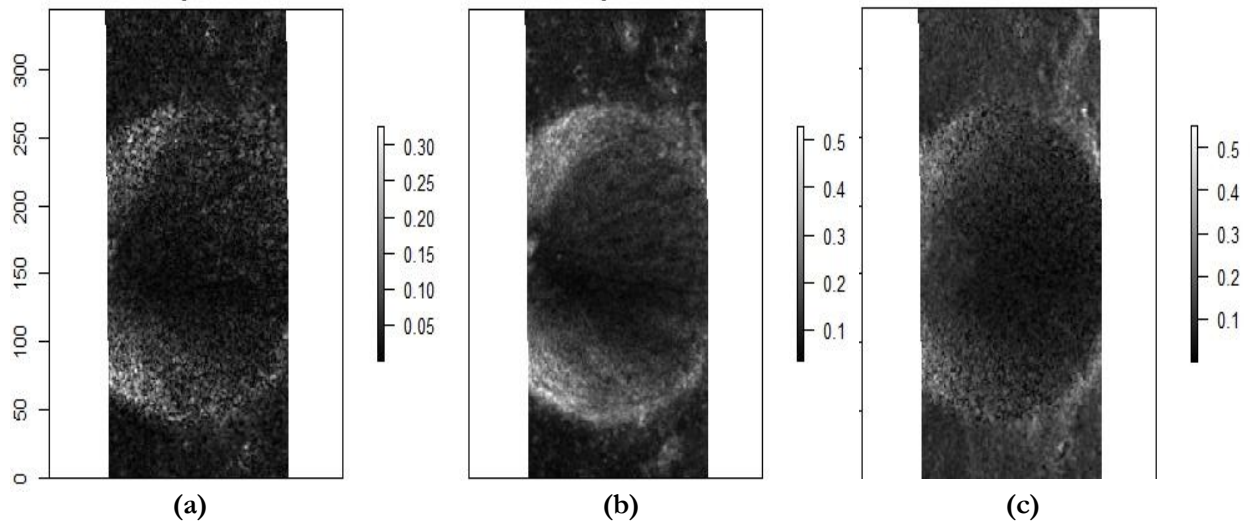
Figure 4-4: Individual scattering components for m-χ decomposition. Each image shows the relative contribution to backscattered power from (a) surface, (b) double bounce and (c) volume scattering mechanisms.

4.3. CPR

CPR for the two study areas is shown in Figure 4-5. High CPR values were observed inside the crater represented in red colour. Studies establish that CPR values of 1 and below relate to lunar regolith and other lunar material while values greater than 1 can relate to volumetric ice deposits. Values which are greater than 1 are also associated with double bounce scattering. This situation is encountered especially when circular polarization is transmitted. Since CPR relates to surface roughness, this ratio increases with increase in surface roughness. The values observed in this research mostly relate to volumetric scattering and very few corresponding to double bounce scattering.

When the two study areas are compared with respect to CPR, anomalously high values greater than one are observed for Erlanger crater, while very few values cross unity for Rozhdestvenskiy crater. The very high values were mostly between 1.5 and 2, while very few crossed the value of 2.5 for Erlanger. As for Rozhdestvenskiy most of the values relate to

lunar regolith with an average CPR of 0.5 except for very few regions represented by light orange to yellow, CPR crosses 1.

Comparison of CPR results with the volume components derived from m-δ and m-χ decompositions can clearly define the regions of volumetric scattering consistent with water-ice deposits. The greater than unity CPR regions of Erlanger crater when evaluated against volume scattering component derived from m-χ decomposition separates or distinguishes CPR values related to double bounce scattering, leaving only those values relating to water-ice deposits.
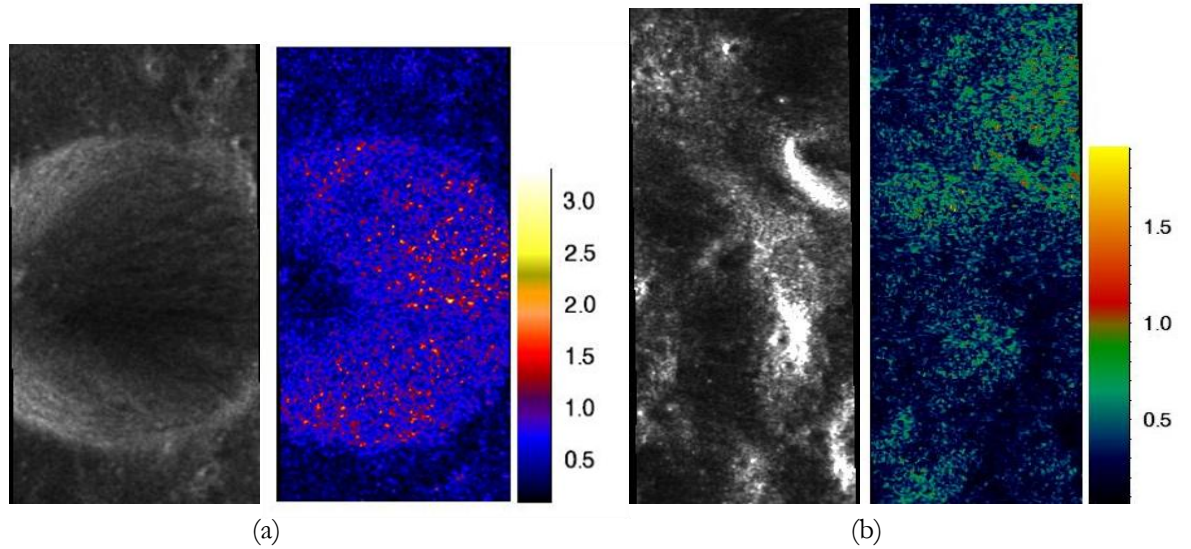
Figure 4-5: CPR images displayed in different colour coding to differentiate areas of CPR greater than and less than unity. (a) The image on the left is the intensity image and corresponding CPR image for Erlanger crater and (b) Rozhdestvenskiy crater.

4.4. Analysis

The analysis was carried out with the help of transects and box plots. Comparisons were made by plotting the values of scattering intensities against the sample number for m-χ and m-δ decompositions. Comparison of individual scattering intensities for each of the decomposition techniques was also conducted, to study how they vary inside and outside the craters. Transects show the variations in the individual scattering components for the selected samples inside and outside the crater, while Comparison of surface and double bounce scattering is conducted for different decomposition techniques.

4.4.1. Transects

Figure 4-6 shows the intensity image for Erlanger crater, and transects selected (red lines) for regions inside and outside the crater. The plot on the right shows the variation in backscatter intensity for the selected transects.
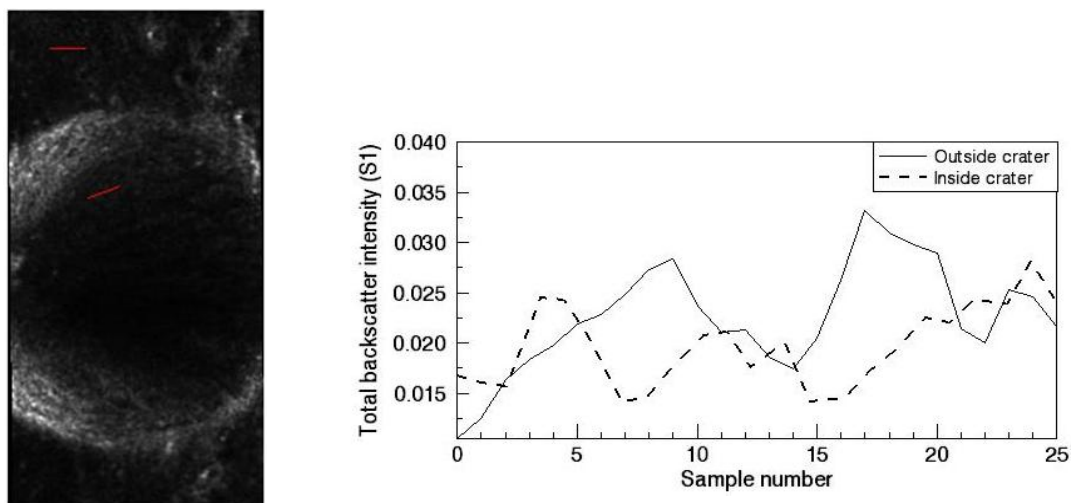
Figure 4-6: Areas selected for analysis sample selected outside and inside the crater are shown in red lines on the intensity image. The plot on the right shows the variation in backscatter intensities for the line transects.
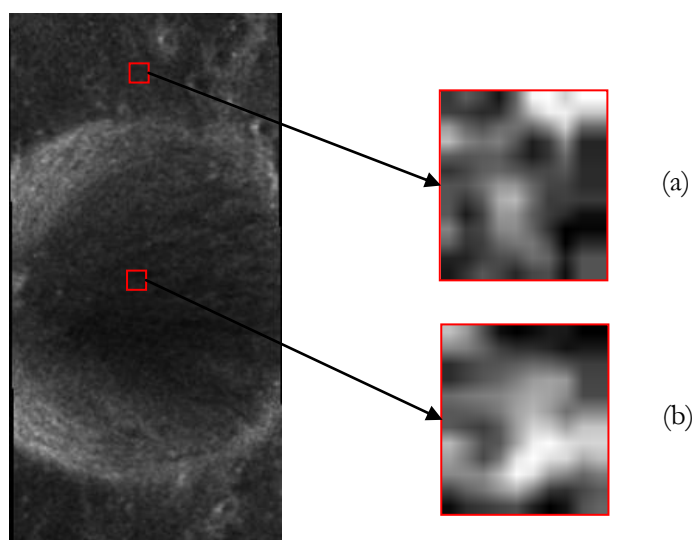
Figure 4-7:Areas selected for analysis (a) sample selected outside the crater and (b) sample selected inside the crater. The image on the left is the intensity image S_1

Figure 4-7 shows the samples selected for box plot analysis. The smoothened effect of the zoomed images (a) and (b) is due to image compression while saving the images.
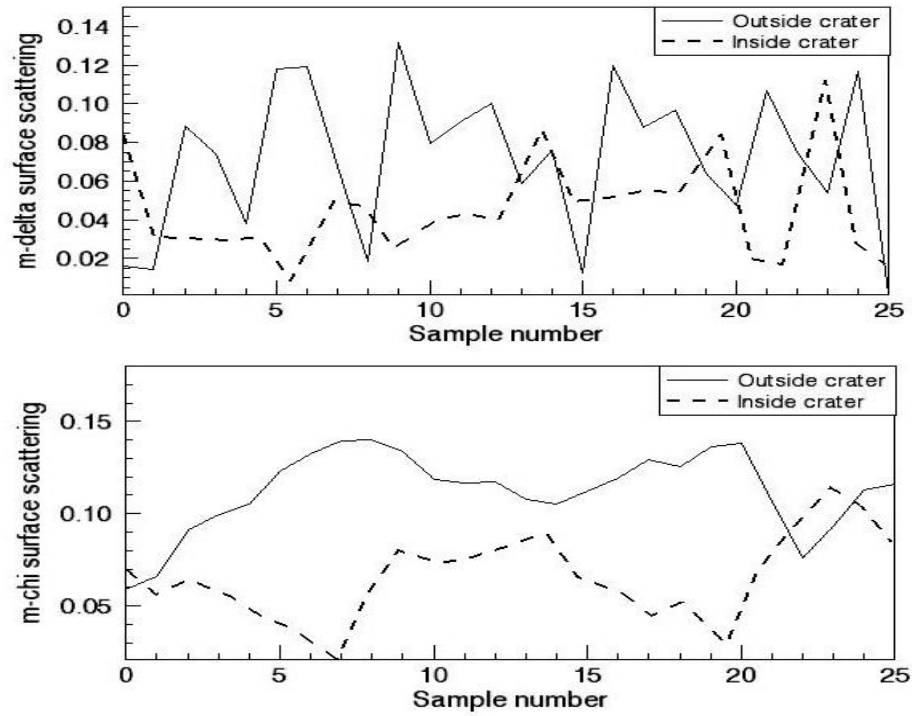
Figure 4-8:Variation in surface scattering component for m-δ (above) and m-χ (below) decompositions for regions outside and inside Erlanger crater

Figure 4-8 shows the variations of relative contribution for intensities in surface scattering derived for regions outside and inside the Erlanger crater for m-δ and m-χ decompositions. Surface scattering component inside the craters is comparatively less than outside the crater for the decompositions. These results comply with scattering possible from the topography pertaining to the lunar surface. Surface scattering is the most prominent type of scattering mechanism encountered on the lunar surface taking in to account the wavelength used. A decrease in the intensity of this component is observed from lunar craters, where the topography changes with respect to the materials present, surface roughness, slope and other factors, which influence the type and intensity of scattering. The difference in surface scattering for varying lunar surface topography is clearly observed in m-χ scattering. The same examined using m-δ decomposition seems to be a little complicated due to the sudden dips corresponding to very little or no contribution from this component, which is highly inappropriate in context of the lunar surface scattering.

The box plots for surface scattering in Figure 4-9 explain the scattering component well and support the observations of the transect plots. It is clearly evident that surface scattering from m-χ decomposition is higher compared to m-δ decomposition. Also, the contribution of this component outside the crater for m-χ decomposition does not have low values as observed from m-δ decomposition (Figure 4-9 (b)).
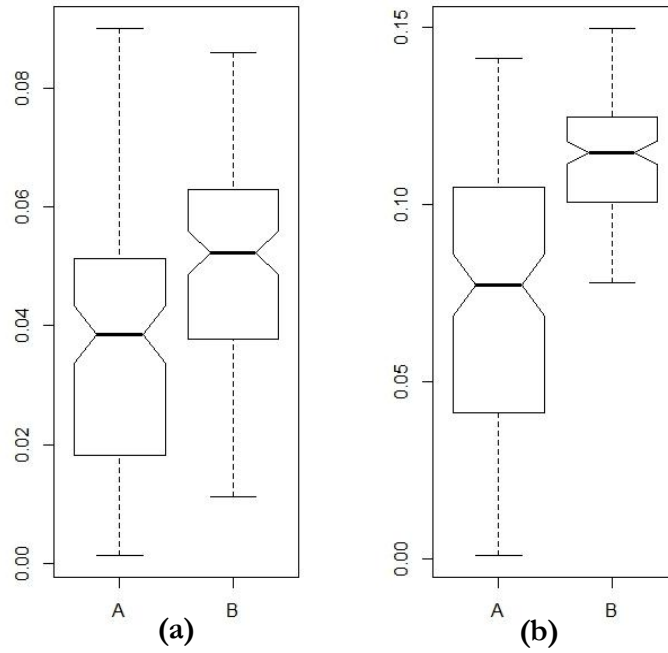
Figure 4-9: Box plots for (a) Inside the crater (b) outside the crater. A and B denote m-δ and m χ decompositions respectively.

Variation in double bounce scattering for the selected transects is shown in Figure 4-11 and the box plots for double bounce scattering components are presented in Figure 4-10. The relative contribution of this mechanism varies for regions inside and outside the craters. The results obtained from the m-δ decomposition differ from that of m-χ decomposition. Greater variations are observed in the m-δ decomposition while this component has more or less similar contribution in the m-χ decomposition. Differences outside and inside the craters in the m-χ decomposition are observed, which could be possible from lunar surface if the surface is highly irregular. This is not the case here as the region from which the sample has been selected is smoother taking into account the wavelength used and general lunar surface composition. The relative contribution of this component for m-δ decomposition is also higher than that derived from the m-χ decomposition.
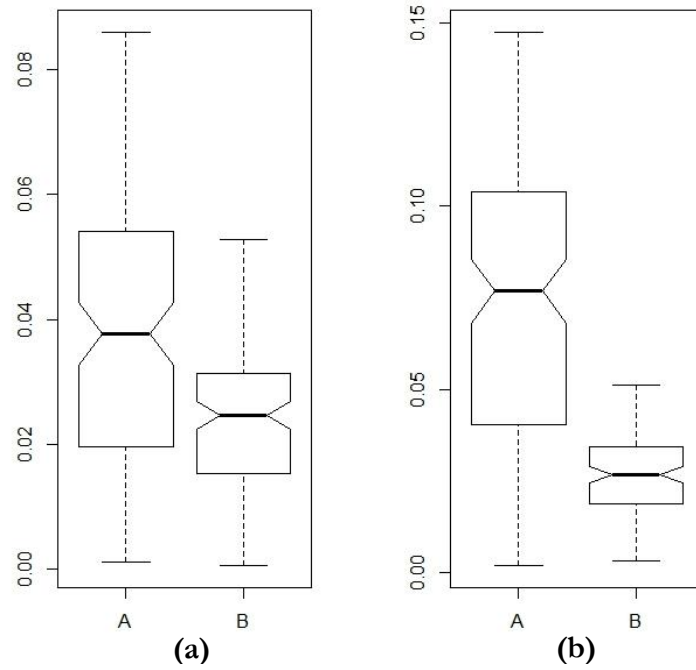
Figure 4-10: Box plots for double bounce scattering for (a) Inside the crater (b) outside the crater. A and B denote m-δ and m-χ decompositions respectively.
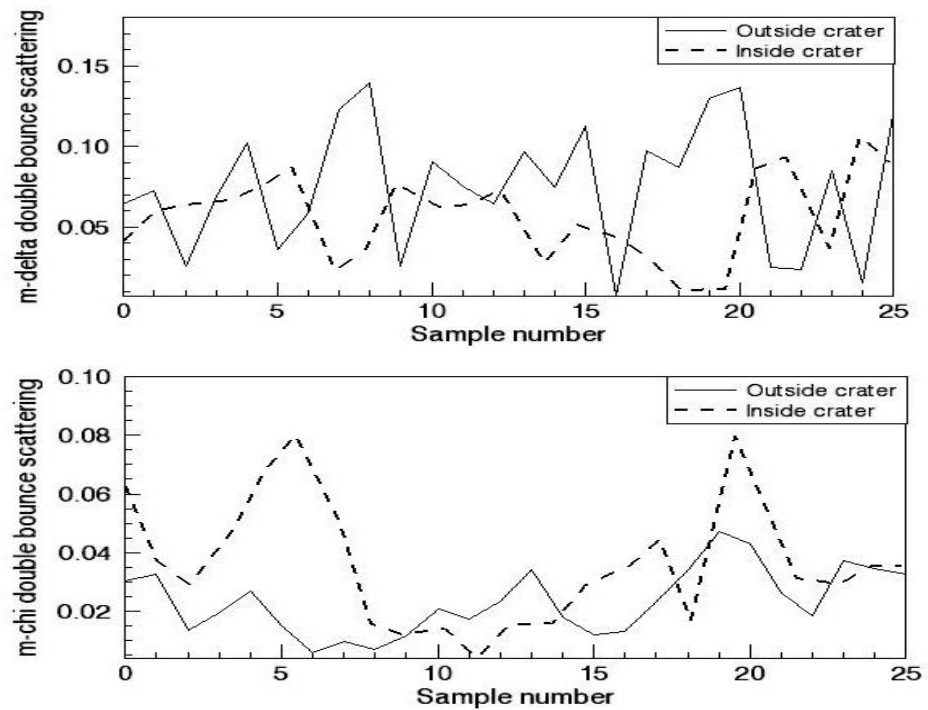
Figure 4-11: Variation in double bounce scattering component for m-δ (above) and m-χ (below) decompositions for regions outside and inside Erlanger crater

Volume scattering for the two decompositions was found to be similar. Therefore, result from m-χ decomposition has been considered to study the fluctuation of volume scattering mechanism for varying topography. The result of the transect plot for samples collected inside and outside the crater has been presented in Figure 4-12. The relative contribution of this mechanism is greater inside the craters than on the outside. The box plots for this component (Figure 4-13) show interesting results. Though the most of values inside the crater have higher values, the mean of both the samples is almost similar. A few pixels outside the crater have very high values show as outliers in the plot.
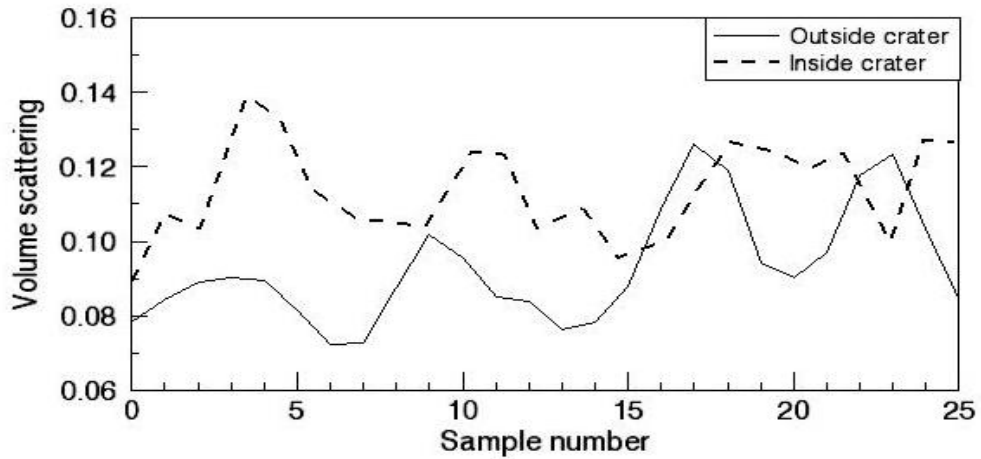
Figure 4-12: Variation in volume scattering for regions outside and inside the Erlanger crater. This component is invariable in m-δ and m-χ decompositions.
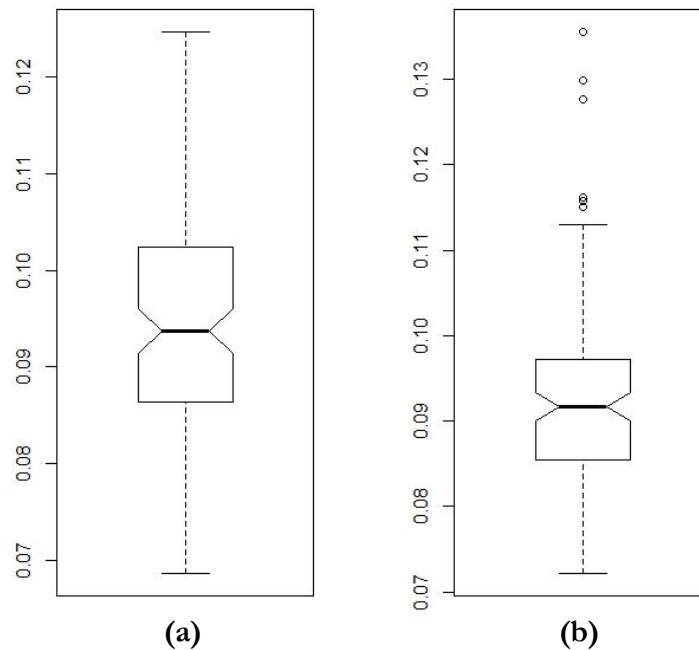
Figure 4-13: Box plots for volume scattering components (a) inside the crater and (b) outside the crater for m-χ decomposition.

4.5. H-α decomposition

The Entropy and mean alpha images for the first study area (Erlanger crater) are shown in Figure 4-14. Regions of high entropy (closer to 1) were observed inside the crater. The regions of high entropy can be identified with the help of red colour from the image Figure 4-14(a). The areas of high entropy represent diffuse type of scattering pertaining to either volume scattering or a combination of surface (diffuse component) and volume scattering (dipole). The $\bar{\alpha}$ values are greater than or equal to 45° for the equivalent high entropy pixels. Low values of entropy denote high degree of polarization and in turn specular surface scattering. Surface scattering is dominant immediately outside the crater and also from the inner wall of the crater from where the Radar backscatter response is very strong. An increase in entropy values indicates the depolarized case, or randomness in the backscattered signal; this clearly implies the case of volume scattering. Blue colour in both the images denotes areas of surface scattering (specular component) as the entropy is low and also the $\bar{\alpha}$ is below 40°. As $\bar{\alpha}$ reaches 45° (green colour), an increase in entropy was observed denoting that the scattering response is not pure but a combination of different type of scatterers.

Figure 4-15 shows the entropy and $\bar{\alpha}$ images for study area two (Rozhdestvenskiy crater). Patterns similar to study area 1 were observed on the floor of the Rozhdestvenskiy crater. Depressions on the crater floor have high entropy values and corresponding $\bar{\alpha}$ values closer to 45° and above. Surface scattering was clearly identified by lower entropy values and low $\bar{\alpha}$ angles. Here, dominance of double bounce and surface scattering was observed, while contribution from volume scattering component was little.
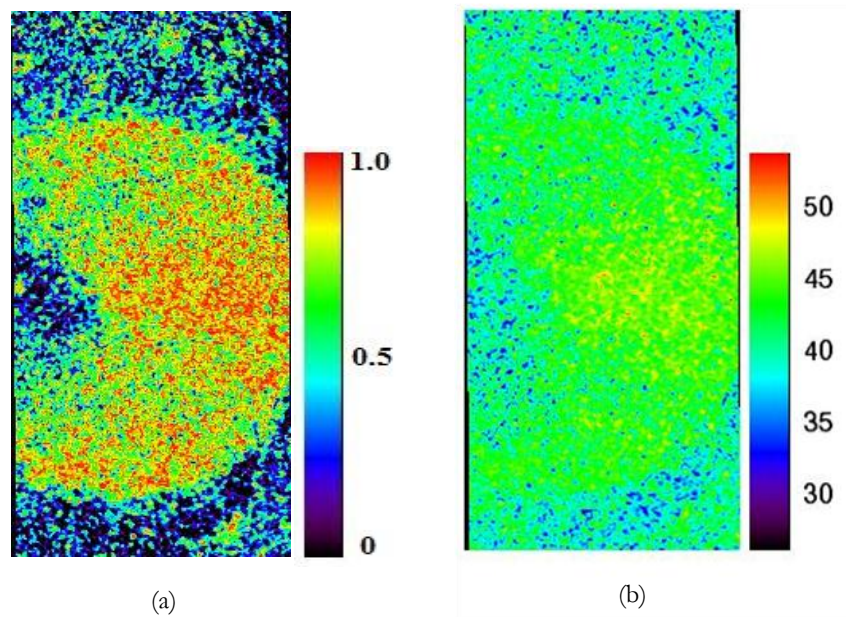
Figure 4-14: The result of H-α decomposition- (a) Entropy (H) and (b) Mean alpha ($\bar{\alpha}$) images.
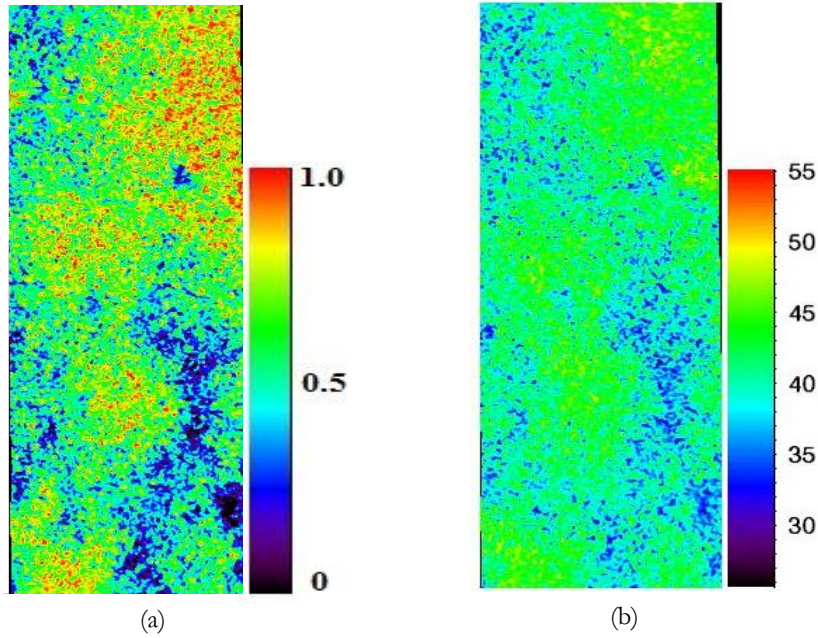
Figure 4-15: (a) Entropy and (b) mean angle alpha images for study area 2. ᾱ values closer to 0° indicate surface scattering, at ᾱ = 45° dipole scattering is dominant while values closer to 90° represent dihedral scattering.

4.6.   H- ᾱ classification plane

Another method to interpret the results of H-α decomposition is by mean dominant scattering mechanism given by the Eigen values and Eigen vectors introduced in Chapter 2. Figure 4-16 shows the scatter plot between H and ᾱ. The plot is divided into 9 zones which can specify the scattering characteristics that are measured by the coherency matrix as specified in [26]. The 2 Eigen values and Eigen vectors obtained in the present case give rise to only two components and hence, it is difficult to extract individual scattering components. An alternative to this is the H/α plane or plot; it describes the type of scattering and scatterer based on the values of H and ᾱ.

Zone 9 is characterized by low entropy scattering with ᾱ values less than 42.5°. As described earlier lower ᾱ values and low entropy indicate surface scattering. Bragg surface scattering and specular scattering fall under this category. On comparison with study area 2, more number of pixels were categorized in the low entropy scattering zone for study area 1. We can also observe this from the intensity images.

Zone 8 represents low entropy dipole scattering. Highly correlated scattering mechanisms which show variations in their received amplitudes are perceived here. Isolated dipole scatters can be identified from this region. Limited number of pixels fall into this category in both the study areas. A very thin line for differentiating Bragg's type of scattering and low entropy dipole scattering can be identified.

Zone 7 shows multiple scattering events caused due to low entropy. This zone corresponds to low entropy double, or even bounce scattering due to the effect of isolated dielectric and metallic dihedral scatterers characterized by $\bar{\alpha}$ values greater than 48°. Few pixels can be identified in this zone for study area 1. These pixels could be false positives or a combination of double bounce and volume scattering.
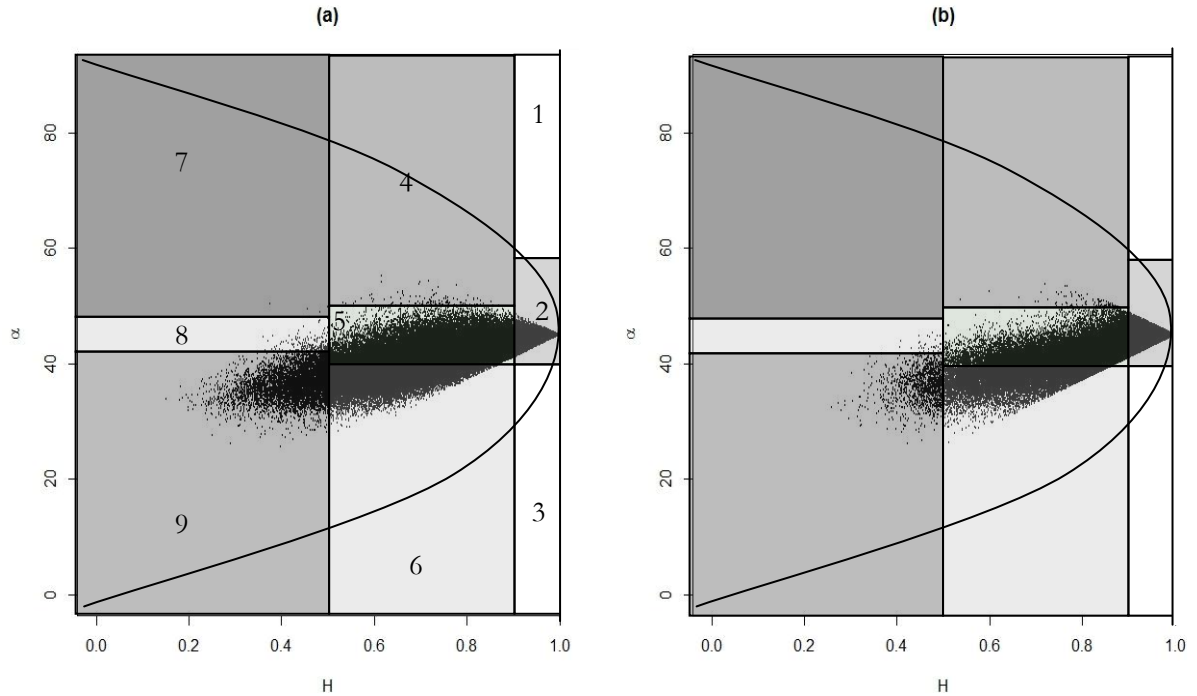
Figure 4-16: H- plane for the two study areas. (a) Erlanger crater (b) Rozhdestvenskiy. Both of them follow a similar trend having very high entropy values.

Zone 6 characterizes the medium entropy surface type of scattering. Increase in entropy in this zone represents changes in surface roughness. This zone is a special case where there is an increase in entropy but $\bar{\alpha}$ angle is less than 42.5°. For the region of Erlanger the pixels of this zone are clustered to the upper left corner denoting a slight dependency with zone 9 and 5. Whereas in Figure 4-16(b), a slight spread in the values was observed. This could be attributed to the highly undulating terrain in study area two, giving rise to medium entropy surface scattering (diffuse component).

Zone 5 indicates medium entropy volume scattering. This zone includes scattering from anisotropic scatterers which give rise to strong dipole scattering. This is the most populated zone for the Erlanger crater and the pixels populate almost the whole zone, indicating strong contribution from volume type of scattering due to the presence of anisotropic medium. In the second plot for Rozhdestvenskiy, though the region is populated compared to other zones, the spread of the values is restricted to the lower half of the region. This could mean a mixture dipole and diffuse surface scattering. A phenomenon that can occur on the lunar surface, as a mixture of surface and subsurface scattering as longer wavelength (12.6 cm) is used.

Zone 4 shows the medium entropy multiple scattering phenomena. Dihedral or double bounce scattering with medium entropy values can be accounted for in this category. On evaluation both the study areas contribute very little to this zone. Double bounce scattering from lunar surface due to the natural orientation of rocks, or surface can be attributed to this type of scattering. As observed from other decomposition techniques described earlier, the results for dihedral scattering seem to comply. The contribution of double bounce scattering from m-δ and m-χ was also observed to be very little.

Zone 3 classifies the high entropy surface scatter. This class is a non-feasible region as it is very difficult to distinguish surface scattering for entropy values greater than 0.9

Zone 2 shows the high entropy volume scattering arising from H>0.9 and $\bar{\alpha}$ at 45°. This type of scattering mostly occurs from highly anisotropic media. Sometimes the extreme behaviour can be attributed to random noise, which indicates completely depolarized signal. The values in this region for both the study areas follow a similar pattern. The values in this zone converge as entropy reaches 1.

Zone 1 characterizes high entropy multiple scattering phenomena. In the H>0.9 region, it is not possible to distinguish double bounce with high entropy. So this category becomes non-feasible for hybrid or dual polarized data.
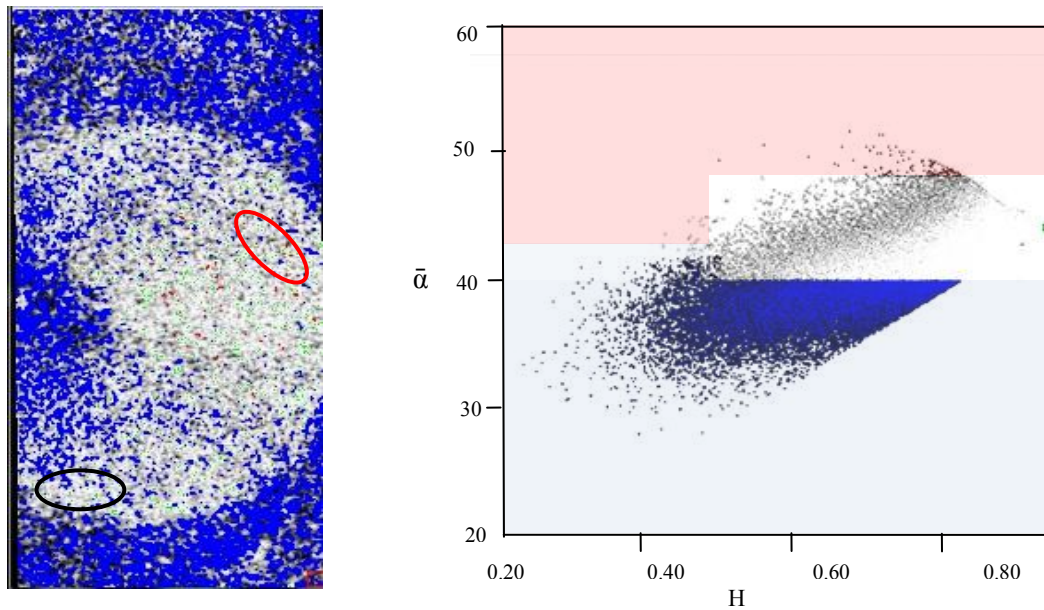
Figure 4-17: Image showing the scattering mechanisms for H-α decomposition. The scatter plot on the right shows the H-α plane. The blue colour stands for surface scattering (both specular and diffuse), red colour for double bounce and the whitish to grey represents volume scattering component.

4.8. Validation

In order to validate the results obtained by applying the H-α decomposition method, the scattering response, and polarization ratios obtained from Greenland ice-sheet and the icy planet of Europa, are taken into account. It has been predicted that on Europa (Jupiter's moon), water- ice is the dominant near surface material and it has the purest ice form. For this purpose readings from Europa have been considered. The interior of Erlanger crater has been selected for the validation purpose as volume scattering was found to be very high there.

The information obtained from literature study related to Radar backscatter properties of ice are presented in Table 4-1.

	CPR (μ_C)	LPR (μ_L)
Greenland ice sheet[47]	>1	>0.3
Icy planets (Europa)[48]	>1	0.42± 0.15
Erlanger	Mean 0.7 and max 2.7 for inside the crater	0.37

Table 4-1: Radar backscatter properties of Greenland ice sheet, Icy planet Europa and the lunar crater Erlanger. The table gives the values of CPR and LPR.

The Greenland ice sheet data has been obtained by flying airborne Radar over the entire Greenland ice sheet. This was obtained for 5.6 and 24 cm wavelengths. The records considered are for Crawford point which is to the west of Greenland and comes under the percolation zone. In the percolation zone, we can find buried solid ice inclusions. The observations for the icy planet Europa have been made at 13 cm wavelength.

The LPR and CPR of reference data comply with the obtained results of the research. Although, the mean CPR inside Erlanger is around 0.7 there exist areas, or clustered pixels highlighted in a red and black ellipse in Figure 4-17, where CPR is greater than unity and at points reaching 2.5. The region in the red and black ellipses contains 1000 pixels each.

Table **4-2** shows the percentage of pixels in the selected regions which fall in three categories. On an average 30 pixels out of 1000 have CPR greater than 1, which might indicate the presence of water-ice deposits. The high CPR values can be attributed to high surface roughness or low subsurface roughness as concluded by Fa *et* al. [21]. If we look closely at the selected regions through the H-α decomposition a combination of scattering mechanisms are observed with a dominance of volume scattering. This might indicate that some of the high CPR's greater than unity can be due to anisotropic buried ice inclusions.

	CPR<1	1≤ CPR ≤2	CPR>2
Red ellipse	65%	34.2%	8%
Black ellipse	72.9%	26.6%	5%

Table 4-2: Percentage of pixels from the selected regions falling under different classes selected for CPR.

This Chapter presented the results obtained by employing different techniques suited for hybrid polarized data. In addition to this, data analysis and validation results have also been presented.

5. DISCUSSIONS

This chapter presents the discussions of the obtained results of the research work carried out. The discussions cover the highlights and the back draws encountered during the execution of the research project.

5.1. Stokes parameters based approach

The concept and importance of Stokes parameters has already been discussed. The Stokes parameters based approach for retrieving scattering information by applying decomposition methods from hybrid polarimetric data has various advantages as discussed in Chapter 2. The results support this statement as, the use Stokes parameters helped in the implementation of H-α decomposition technique. The data format for mini-SAR being orthogonal linear receive in the H and V polarization and the cross product between H and V, each of the Stokes parameters can successfully be retrieved. From the backscatter values represents by Stokes parameters, other important parameters can then be retrieved based on which interpretations and analysis could be conducted. The general coherency and covariance matrix based decomposition techniques approach falls short in this scenario as the dimension of the coherency matrix is 2×2 in this case. Therefore, the Stokes parameters present an efficient way for retrieving polarimetric information from hybrid polarity data.

5.2. The m-δ, m-χ, H- α decompositions and CPR

The present research focuses on retrieving scattering information by applying an Eigen vector based H-α decomposition technique. In addition to this, the implementation of the m-δ and m-χ decomposition techniques has also been discussed. The three decomposition techniques were evaluated against each other for finding out a method, best fit for retrieving scattering information from hybrid polarimetric data. Additionally, CPR has been used as supplementary information to aid the interpretation of the results. The m-δ decomposition was weaker in differentiating between odd bounce and even bounce scattering compared to the m-χ technique. In the H-α classification plane, the boundaries for separating the scattering mechanisms are subjective, i.e. they are based on general properties of scattering mechanisms and are not inherent to a particular data set. The three techniques were evaluated based on their success in retrieving the three scattering components.

5.2.1. Surface scattering

The analysis of surface scattering from m-δ and m-χ decompositions showed a great deal of variation for regions inside and outside the crater. Adjacent pixels which are generally spatially correlated have cell values which are also correlated except for boundary pixels for two different classes/features. For the lunar surface the classes do not change as drastically as we can find on Earth (example land and water). The m-χ decomposition showed a smother

variation in this context while in the m-δ the changes were drastic. The m-χ decomposition was found to be more realistic compared to the m-δ decomposition. While these two decomposition techniques helped in finding the relative contribution of the scattering mechanisms in a broad sense, the H-α decomposition and the H-α plane helped to classify the pixels not only based on the scattering type but also in providing information about the target leading to the particular scattering scenario. In addition to this, the intensity of surface scattering was found to be greatest along the left wall of the crater, which is directly perpendicular to the incoming Radar signal. The total backscattered power for this region was also considerably high when compared with regions inside the crater.
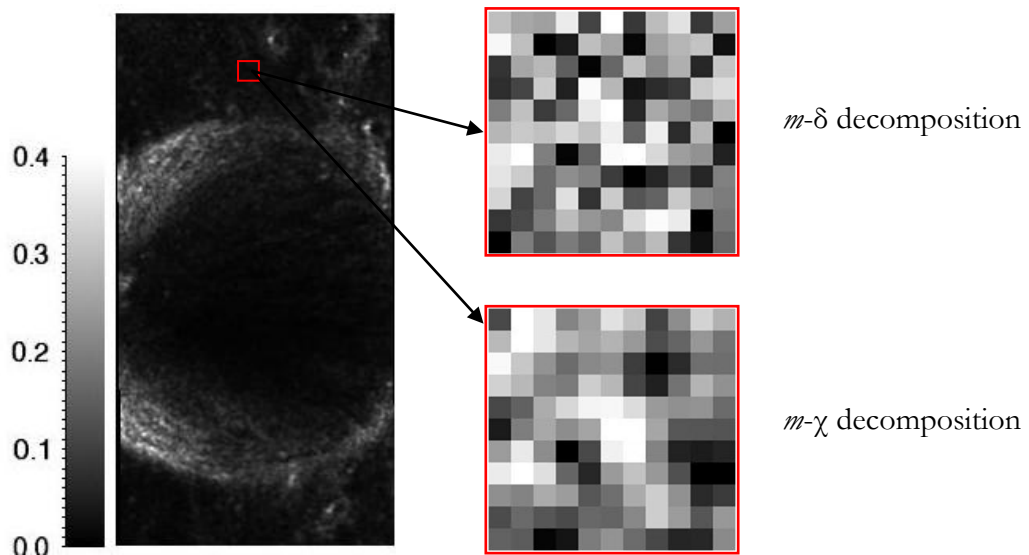
Figure 5-1: The image on the left is the intensity image and the red box shows the sample selected for analysis. The images on the right show the surface scattering component for m-δ decomposition and m-χ decomposition.
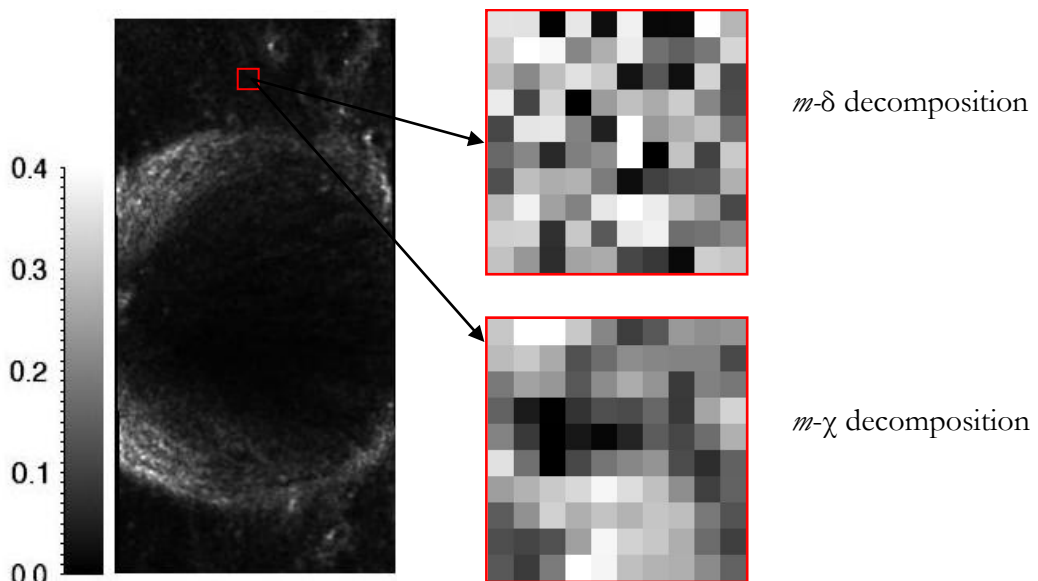
Figure 5-2: The images on the right show the double bounce scattering component for m-δ decomposition and m-χ decompositions. The image of the m-δ decomposition gives chess board like look while the variations in m-χ decomposition are transitional.

5.2.2. Double bounce scattering

A trend similar to that of surface scattering was observed with double bounce scattering too. When m-δ decomposition has been used drastic change in the pixels values was observed for spatially correlated pixels while the contribution from m-χ decomposition was found to be connected in a better way.

Although it is easy to identify the pixels contributing to double bounce scattering mechanism it is difficult to analyze the variations in this mechanism for H-α decomposition. Most of the double bounce scattering was identified along the crater rim and inside the crater, or when the topography is such that it forms a natural dihedral. Double bounce scattering was better categorized using the m-χ decomposition rather than m-δ or H-α method.

5.2.3. Volume scattering

Volume scattering is the most important identifier of volumetric ice deposits. This component is similar for the m-δ and m-χ decompositions. Most of the pixels had a volume scattering component associated with them in the two decompositions. Volume scattering was predominantly higher inside the crater region than on the outside. Even for the area of Rozhdestvenskiy, the secondary craters were consistent with volume scattering. The characteristic volume scattering from inside the craters can be assigned to buried rocks, voids or water-ice deposits in the subsurface. An interesting output of the research was the identification of volume scattering in an enhanced manner with the help of H-α decomposition. Anisotropic targets which could lead to dipole scattering were recognized and the results of this complied with those of m-δ, m-χ decompositions and CPR.

5.3. Comparison with Other studies

CPR based analysis of the results suggest high volume scattering taking place inside the crater. There also has been a record CPR values as high as 2.5 and 3 from inside the Erlanger crater. This is where ambiguity arises, whether these values correspond to ice-deposits or are they due to high double bounce scattering. This ambiguity was resolved by

- Masking out CPR values less than 1
- Comparing CPR>1 to the volume and double bounce scattering obtained by H-α decomposition.
- Reaffirming the results by taking into account the m-χ decomposition results.

The backscatter values obtained for reference data were in $\sigma°$ (backscattering coefficients) while those for mini-SAR were in $\beta°$. Therefore it was difficult to compare the backscatter coefficients. The ratios CPR and LPR were observed to be unvarying under the backscatter

coefficient considered (σ° or β°). Therefore, CPR and LPR were compared for the obtained and reference datasets.

The results presented in this research work pertain to the lunar North Polar Region, the same techniques applied to data obtained from the equatorial and South Polar Region may differ. The differences may arise due to the topographic and physical conditions (temperature, surface roughness, etc.) present there.

5.4. Speckle and geometric distortions

The natural scattering characteristics of each pixel are affected by speckle filtering and other averaging processes. Application of filters or averaging process could degrade the quality of information being retrieved using the decomposition methods. Studies state that entropy, and the averaged alpha angle are dependent on the averaging process [26]. Entropy value was observed to increase with the amount of averaging but it had less affect on mean angle alpha ($\bar{\alpha}$). Retrieving polarimetric information and studying the scattering scenarios being the objective, speckle filters have not been applied in this research. Since the dataset used in this research is processed till level 2, where multi-look process has already been conducted, the effect of speckle has been assumed to have minimum effect. Additional filters have not been applied to avoid loss of spatial information.

Inherent characteristics of a Radar image include layover, foreshortening and Radar shadow. For low angles of incidence(case of mini-SAR), the effect of layover and foreshortening is negligible, although there can be some contribution from Radar shadows [1], [26]. Although, these phenomena are identified to occur in the crater regions, since the topographic effects are not too severe, these geometric distortions actually enhance the visual appearance of relief and terrain structure. Sometimes these characteristics make Radar imagery very useful for applications such as topographic mapping and identifying geologic structures. Topographic corrections when applied can help in locating the areas of water-ice deposits and enhance the quality of information [49]. These effects have not been compensated for in this work.

6.   CONCLUSIONS

This chapter gives the conclusions of the research work carried out. The research questions posed to achieve the objective are answered. This is followed by recommendations for future work.

6.1.   What are the differences and similarities between the m-δ and m-χ decompositions and what is their success in retrieving the scattering information?

The two decompositions were successful in retrieving the scattering mechanisms from hybrid polarity data. The results of the decomposition provided relative contribution of each scattering mechanism. Though, these techniques provide the scattering information, their success in providing target information is quite low. We require additional information like CPR or intensity in order to understand the target characteristics with the information provided by the decompositions. The differences in the decomposition results arise due to the parameters taken into account for the decomposition. δ describes the phase difference and is very sensitive to minor changes in the topography and hence creates confusion between spatially correlated pixels. On the other hand, χ the ellipticity parameter differentiates the scattering mechanisms based on the sign of χ.

The decompositions differ in terms of surface and double bounce scattering scenarios as shown in the results section. The volume scattering component remains the same in both the decompositions. This can be attributed to the criteria established to categorize this mechanism. The criterion is set such that contribution of volume scattering is the product of the total intensity of the backscatter and the degree of depolarization or entropy. The greater the randomness in the signal greater is the contribution from volume scattering component.

6.2.   How to apply the H- α decomposition technique to hybrid polarity data?

The objective of the research is checking the feasibility of applying H-α technique to hybrid polarity data and hence this question is very significant. This Eigen vector decomposition technique was employed from [23], [40] and was made to fit the hybrid polarization data format. A 2×2 coherency matrix of the backscatter field was generated and then the matrix was decomposed as a combination of normalized Eigen values and Eigen vectors. The derivation of Eigen values was easy as they are dependent on the degree of polarization in the 2×2 coherency matrix problem. In addition, since there are only 2 Eigen values the principle of orthogonality was applied to derive the second Eigen value. Finally from the Eigen values and Eigen vectors we obtain the entropy and alpha parameterization of the coherency matrix.

6.3.   Does the derived information enhance the findings of CPR?

The information retrieved from the H-α decomposition gives the type of scattering that is taking place and the H-α plane enhances this information further by giving an insight into the target properties. Whether these properties relate to particular targets is a difficult question to answer as field data is not available for validation purposes. High dipole scattering from anisotropic particles was encountered, which might indicate the presence of water ice. This information alone is not sufficient for characterizing or detecting water-ice deposits from the lunar surface. Although this technique alone cannot be successful in detecting water-ice deposits, it can definitely enhance the findings of CPR. The ambiguity in caused in analysis CPR for values greater than unity can be reduced by the complementary information from the H-α decomposition technique in characterizing lunar backscatter.

6.4.   Does the H-α technique help in providing better results in terms of amount of scattering information retrieved compared to CPR and the m-χ, m-δ decomposition techniques?

The H-α technique helped in categorizing the scattering mechanisms and also in providing information on the target properties. The latter is an additional feature that is not available from the m-δ and m-χ decomposition techniques. Due to the constraint in the data format, estimation of mean dominant scattering mechanism was not possible from the H-α technique and therefore calculation of relative contribution from each mechanism to the total backscatter was not carried out. This was possible form the other two decomposition techniques. It is difficult to distinguish the scattering type from CPR, though insight could be provided on the relative surface roughness, causing variations in CPR.

6.5.   How to validate the results obtained by using literature?

Validation of the results was a challenge in itself. Literature based validation requires a wide range of survey of previous studies that have been conducted. Results obtained from previous studies on lunar surface using Radar polarimetry are ambiguous, since some of them were predictions or assumptions. For the purpose of validation Radar polarization ratios form Greenland ice sheet and the polarization ratios from Europa have been treated as reference data. The validation results have been presented in Section 4.8 of Chapter 4.

In conclusion, polarized Radar backscatter for mini-SAR is mostly dominated by scattering from the surface and shallow buried rocks (subsurface interactions), while the depolarized Radar backscatter is dominated by scattering from subsurface interactions causing volume type of scattering.

The research work presented an alternative to explore hybrid-polarimetric data. The Eigen vector based H-α decomposition technique was applied successfully to a relatively new data format. The results obtained can be utilized for various applications such as classification of targets. The H-α technique offers an alternative to the m-χ and m-δ decomposition techniques. In addition, the results also enhance the findings of CPR, thus providing a more robust tool for prediction or detection of water-ice deposits.

6.6.   Recommendations

Taking into account the results obtained from this research, following recommendations are made considering the future prospects

- The data from mini-SAR and mini-RF is available in a new format which is not readable in most of Radar image processing software. The ISIS software which is designed for processing of planetary data has a complex interface and is operable only on LINUX OS. Therefore most of the processing had to be done manually. The recommendation is to use ISIS if one is familiar with the LINUX interface and coding. This could cut down the manual labor and the processing time.

- The 2×2 coherency matrix could be converted into a 3×3 pseudo scattering/coherency matrix and the decomposition techniques could be implemented. This would allow the derivation of mean dominant scattering mechanism from the H-α decomposition method.

- Considering the dielectric properties along with the decomposition results could improve the findings of water-ice deposits and could support the findings of CPR.

- Topographic corrections with the help of DEM or InSAR techniques could provide a better insight and also help in locating the positions of potential water-ice deposits.

- Availability of full-polarized data could characterize the lunar backscatter in an efficient way. The lack of field data poses a constraint in the research for validation purposes. A more robust method for validation is another alternative to carry the research forward.

REFERENCES

[1]   I. H. Woodhouse, *Introduction to Microwave Remote Sensing*. Taylor&Francis, 2006.

[2]   D. Lusch, *Introduction to Microwave Remote Sensing*. Centre for Remote Sensing, Michigan State University, 1999.

[3]   N. J. S. Stacy, "Arecibo Radar Mapping of the Lunar Poles: A Search for Ice Deposits," *Science*, vol. 276, no. 5318, pp. 1527–1530, 1997.

[4]   K. Watson, B. Murray, and H. Brown, "On the possible presence of ice on the Moon," *Journal of Geophysical Research*, vol. 66, no. 5, pp. 1598–1600, 1961.

[5]   K. Watson, B. C. Murray, and H. Brown, "The behavior of volatiles on the lunar surface," *Journal of Geophysical Research*, vol. 66, no. 9, pp. 3033–3045, 1961.

[6]   J. R. Arnold, "Ice in the lunar polar regions," *Journal of Geophysical Research: Solid Earth*, vol. 84, no. B10, pp. 5659–5668, 1979.

[7]   W. Fa and Y.-Q. Jin, "A primary analysis of microwave brightness temperature of lunar surface from Chang-E 1 multi-channel radiometer observation and inversion of regolith layer thickness," *Icarus*, vol. 207, no. 2, pp. 605–615, 2010.

[8]   P. Lucey, "Understanding the Lunar Surface and Space-Moon Interactions," *Reviews in Mineralogy and Geochemistry*, vol. 60, no. 1, pp. 83–219, 2006.

[9]   P. Spudis, "Introduction to the Moon," *Moon 101 Lecture Series*. [Online]. Available: http://www.spudislunarresources.com/moon101.htm. [Accessed: 09-Nov-2012].

[10]   "Light as a Wave | Las Cumbres Observatory Global Telescope Network." [Online]. Available: http://lcogt.net/spacebook/light-wave. [Accessed: 10-Jan-2013].

[11]   "EDU.Photonics.com."   [Online].   Available: http://www.photonics.com/edu/m/Handbook.aspx?AID=25153. [Accessed: 10-Jan-2013].

[12]   R. K. Raney, P. D. Spudis, B. Bussey, J. Crusan, J. R. Jensen, W. Marinelli, P. McKerracher, C. Neish, M. Palsetia, R. Schulze, H. B. Sequeira, and H. Winters, "The Lunar Mini-RF Radars: Hybrid Polarimetric Architecture and Initial Results," *Proceedings of the IEEE*, vol. 99, no. 5, pp. 808–823, 2011.

[13]   R. K. Raney, "Hybrid-Polarity SAR Architecture," *IEEE Transactions on Geoscience and Remote Sensing,*, vol. 45, no. 11, pp. 3397 –3404, 2007.

[14]   N. R. C. Government of Canada, "Tutorial: Radar Polarimetry | Earth Sciences," 07-Feb-2007.   [Online].   Available: http://www.nrcan.gc.ca/earth-sciences/geography-boundary/remote-sensing/radar/1893. [Accessed: 30-Nov-2012].

[15] F. J. Charbonneau, B. Brisco, R. K. Raney, H. McNairn, C. Liu, P. W. Vachon, J. Shang, R. DeAbreu, C. Champagne, A. Merzouki, and others, "Compact polarimetry overview and applications assessment," *Canadian Journal of Remote Sensing*, vol. 36, no. S2, pp. 298–315, 2010.

[16] R. K. Raney, J. T. S. Cahill, G. W. Patterson, and D. B. J. Bussey, "The m-chi decomposition of hybrid dual-polarimetric radar data with application to lunar craters," *Journal of Geophysical Research: Planets*, vol. 117, no. E5, 2012.

[17] N. R. C. Government of Canada, "Radar Polarimetry | Earth Sciences," 29-Jan-2008. [Online]. Available: http://www.nrcan.gc.ca/earth-sciences/geography-boundary/remote-sensing/fundamentals/1025. [Accessed: 30-Nov-2012].

[18] L. M. Carter, D. B. Campbell, and B. A. Campbell, "Geologic Studies of Planetary Surfaces Using Radar Polarimetric Imaging," *Proceedings of the IEEE*, vol. 99, no. 5, pp. 770–782, 2011.

[19] S. Nozette, C. L. Lichtenberg, P. Spudis, R. Bonner, W. Ort, E. Malaret, M. Robinson, and E. M. Shoemaker, "The Clementine Bistatic Radar Experiment," *Science*, vol. 274, no. 5292, pp. 1495–1498, 1996.

[20] S. Mohan, A. Das, and M. Chakraborty, "Studies of polarimetric properties of lunar surface using Mini-SAR data," *Current Science*, vol. 101, no. 2, pp. 159–164, 2011.

[21] W. Fa, M. A. Wieczorek, and E. Heggy, "Modeling polarimetric radar scattering from the lunar surface: Study on the effect of physical properties of the regolith layer," *J. Geophys. Res.*, vol. 116, no. E03005, p. 33 PP, 2011.

[22] T. W. Thompson, E. A. Ustinov, and E. Heggy, "Modeling radar scattering from icy lunar regoliths at 13 cm and 4 cm wavelengths," *J. Geophys. Res.*, vol. 116, p. 27 PP., 2011.

[23] S. Cloude, *Polarisation: Applications in Remote Sensing*. Oxford University Press, USA, 2009.

[24] C. O.P.N, "Applications of Microwaves in Remote Sensing," *International Journal of Computer Applications - IJCA*, 2011.

[25] W. M. Boerner, W. L. Yan, A. Q. Xi, and Y. Yamaguchi, "Basic concepts of radar polarimetry," *Proc. NATO Adv. Res. Worksh. Dir. Inv. Meth. Radar Polar*, 1988.

[26] J.-S. Lee and E. Pottier, *Polarimetric Radar Imaging: From Basics to Applications*, 1st ed. CRC Press, 2009.

[27] North Atlantic Treaty Organization. Research and Technology Organization. Sensors and Electronics Technology Panel. Lecture series, "Radar polarimetry and interferometry La polarimétrie et l'interférométrie radar.," 2007.

[28] W. M. Boerner, "Basics of SAR polarimetry 1," *Radar Polarimetry and Interferometry . Educational Notes RTO-EN-SET-081bis, Paper 3.*, pp. 3–40, 2007.

[29] F. M. Henderson and A. J. Lewis, Eds., *Imaging Radar (Manual of Remote Sensing, Volume 2) 3rd Edition*, 3rd ed. Wiley, 1998.

[30] A. Fung and F. T. Ulaby, "Matter-Energy Interaction in the Microwave Region," *Manual of Remote Sensing*, vol. 1, 1983.

[31] E. Collett, *Field Guide to Polarization*, vol. 05. 1000 20th Street, Bellingham, WA 98227-0010 USA: SPIE, 2005.

[32] Y. Shkuratov, V. Kaydash, V. Korokhin, Y. Velikodsky, N. Opanasenko, and G. Videen, "Optical measurements of the Moon as a tool to study its surface," *Planetary and Space Science*, vol. 59, no. 13, pp. 1326–1371, 2011.

[33] D. B. J. Bussey, P. D. Spudis, and M. S. Robinson, "Illumination conditions at the lunar South Pole," *Geophysical Research Letters*, vol. 26, no. 9, p. 1187, 1999.

[34] B. A. Campbell, L. M. Carter, D. B. Campbell, M. Nolan, J. Chandler, R. R. Ghent, B. Ray Hawke, R. F. Anderson, and K. Wells, "Earth-based 12.6-cm wavelength radar mapping of the Moon: New views of impact melt distribution and mare physical properties," *Icarus*, vol. 208, no. 2, pp. 565–573, 2010.

[35] I. A. Crawford, M. Anand, C. S. Cockell, H. Falcke, D. A. Green, R. Jaumann, and M. A. Wieczorek, "Back to the Moon: The scientific rationale for resuming lunar surface exploration," *Planetary and Space Science*, vol. 74, no. 1, pp. 3–14, 2012.

[36] N. J. S. Stacy and D. B. Campbell, "Stokes vector analysis of lunar radar backscatter," in *Geoscience and Remote Sensing Symposium, 1993. IGARSS '93. Better Understanding of Earth Environment.*, 1993, pp. 30 –32 vol.1.

[37] B. J. Thomson, P. D. Spudis, D. B. J. Bussey, L. Carter, R. L. Kirk, C. Neish, G. Patterson, R. K. Raney, H. Winters, and M.-R. Team, "Roughness and Radar Polarimetry of Lunar Polar Craters: Testing for Ice Deposits," in *Lunar and Planetary Institute Science Conference Abstracts*, 2010, vol. 41, p. 2176.

[38] S. Saran, A. Das, S. Mohan, and M. Chakraborty, "Study of scattering characteristics of lunar equatorial region using Chandrayaan-1 Mini-SAR polarimetric data," *Planetary and Space Science*, vol. 71, no. 1, pp. 18–30, 2012.

[39] R. K. Raney, "Decomposition of hybrid-polarity SAR data," in *PolIn-SAR 2007: Proceedings of the 3rd International Workshop on Science and Applications*, 2007, pp. 22–26.

[40] S. R. Cloude, "The dual polarization H/alpha decomposition," in *Third ESA Workshop on Polarimetry and Polarimetric Interferometry*, Frascati, Italy, 2007.

[41] S. R. Cloude, D. G. Goodenough, and H. Chen, "Compact Decomposition Theory," *IEEE Geoscience and Remote Sensing Letters*, vol. 9, no. 1, pp. 28 –32, 2012.

[42] E. Pottier, J. S. Lee, and L. Ferro-Famil, "Advanced Polarimetric Concepts-Part 1 (Polarimetric Target Description, Speckle filtering and Decomposition Theorems)," DTIC Document, 2007.

[43] "PDS Geosciences Node, Washington University, St. Louis, Missouri." [Online]. Available: http://pds-geosciences.wustl.edu/. [Accessed: 16-Aug-2012].

[44] "Lunar Orbital Data Explorer - Home Page." [Online]. Available: http://ode.rsl.wustl.edu/moon/. [Accessed: 07-Dec-2012].

[45] "Eternal Darkness Near the North Pole - LROC News System," *Lunar Reconnaissance Orbiter Camera*. [Online]. Available: lroc.sese.asu.edu/news/index.php?/archives/95-Eternal-Darkness-Near-the-North-Pole.html. [Accessed: 01-Feb-2013].

[46] "NASA - Image of the crater Erlanger." [Online]. Available: http://www.nasa.gov/mission_pages/Mini-RF/multimedia/erlanger_crater.html. [Accessed: 01-Feb-2013].

[47] E. J. Rignot, S. J. Ostro, J. J. Van Zyl, and K. C. Jezek, "Unusual radar echoes from the greenland ice sheet.," *Science (New York, NY)*, vol. 261, no. 5129, p. 1710, 1993.

[48] G. J. Black, D. B. Campbell, and P. D. Nicholson, "Icy Galilean satellites: Modeling radar reflectivities as a coherent backscatter effect," *Icarus*, vol. 151, no. 2, pp. 167–180, 2001.

[49] B. J. Thomson, D. B. J. Bussey, C. D. Neish, J. T. S. Cahill, E. Heggy, R. L. Kirk, G. W. Patterson, R. K. Raney, P. D. Spudis, T. W. Thompson, and E. A. Ustinov, "An upper limit for ice in Shackleton crater as revealed by LRO Mini-RF orbital radar," *Geophysical Research Letters*, vol. 39, no. 14, 2012.